USP22 drives tumor immune evasion and checkpoint blockade resistance through EZH2-mediated epigenetic silencing of MHC-I

Kun Liu¹, Radhika Iyer¹, Yi Li², Jun Zhu², Zhaomeng Cai¹, Juncheng Wei ³, Yang Cheng¹, Amy Tang¹, Hai Wang¹, Qiong Gao¹, Nikita Lavanya Mani¹, Noah Marx¹, Beixue Gao¹, D. Martin Watterson⁴, Seema A. Khan⁵, William J Gradishar ⁶, Huiping Liu ^{4, 7} and Deyu Fang^{1*}

- 1. Department of Pathology, Robert H. Lurie Comprehensive Cancer Center and Center for Human Immunology, Northwestern University Feinberg School of Medicine, Chicago, IL, 60611, United States.
 - 2. Department of Oncology, 920th Hospital of Joint Logistics Support Force, Kunming, China.
- Center of Metabolic Disease Research, Department of Cardiovascular Sciences, Temple University
 Lewis Katz School of Medicine, Philadelphia, PA, 19140, USA.
- Department of Pharmacology, Feinberg School of Medicine Northwestern University, Chicago, IL,
 60611, United States.
- 5. Division of Breast Surgery, Robert H. Lurie Comprehensive Cancer Center, Feinberg School of Medicine, Northwestern University, 303 E Superior, 4-220, Chicago, IL 60611, USA.
- 6. Division of Hematology/Oncology, Department of Medicine, Feinberg School of Medicine, Northwestern University, Chicago, Illinois.
- 7. Department of Medicine, Division of Hematology and Oncology, Northwestern University Feinberg School of Medicine, Chicago, Illinois.

Key words: USP22, ubiquitination, EZH2, epigenetic regulation, MHC-I, ICB resistance.

Running title: Targeting USP22 overcomes ICB resistance.

Conflicts of interest

Drs. Deyu Fang and Huiping Liu are co-founders and equity owners of ExoMira Medicine Inc. Dr. Fang is the inventor of USP22 inhibitor-S02 (*US patent: 18/556,534*).

Correspondence: Dr. Deyu Fang, 303 E Chicago Avenue, Chicago, IL, 60611, United States.

Northwestern University Feinberg School of Medicine. (Tel: 3125033021) fangd@northwestern.edu.

Abstract

While immune checkpoint blockade (ICB) therapy has revolutionized the antitumor therapeutic landscape, it remains successful in only a small subset of cancer patients. Poor or loss of MHC-I expression has been implicated as a common mechanism of ICB resistance. Yet the molecular mechanisms underlying impaired MHC-I remain to be fully elucidated. Herein, we identified USP22 as a critical factor responsible for ICB resistance through suppressing MHC-I-mediated neoantigen presentation to CD8 T cells. Both genetic and pharmacologic USP22 inhibition increased immunogenicity and overcome anti-PD-1 immunotherapeutic resistance. At the molecular level, USP22 functions as a deubiquitinase for the methyltransferase EZH2, leading to transcriptional silencing of MHC-I gene expression. Targeted *Usp22* inhibition resulted in increased tumoral MHC-I expression and consequently enhanced CD8 T cell killing, which was largely abrogated by *Ezh2* reconstitution. Multiplexed immunofluorescence staining detected a strong reverse correlation between USP22 expression and both β2M expression and CD8⁺ T lymphocyte infiltration in solid tumors. Importantly, USP22 upregulation was associated with ICB immunotherapeutic resistance in patients with lung cancer. Collectively, this study highlights the role of USP22 as a diagnostic biomarker for ICB resistance and provides a potential therapeutic avenue to overcome the current ICB resistance through inhibition of USP22.

Introduction

Immune checkpoint blockade (ICB) therapy works by disrupting inhibitory signals thereby preventing T cell activation and has shown remarkable success in cancer treatment (1). However, the success rate of ICB therapy remains limited to a small fraction of patients (2). The efficacy of ICB therapy relies on cytotoxic CD8* T-cell (CTL) recognition of neoantigens presented on major histocompatibility complexes (MHC) class I, which comprises of a heavy-chain and beta-2-microglobulin (*B2m*) (3). An important mechanism that cancer cells have evolved to escape antigen presentation is the downregulation or absence of MHC class I expression. This weak MHC class I expression leads to a lack of antigen presentation to recruit and activate CD8* cytotoxic T lymphocytes and could explain the limited efficiency of ICB therapy (4). Consequently, aberrant expression of key components within MHC-I antigen-processing and presentation are frequently observed across various human cancers, posing a significant barrier to ICB effectiveness in treating many, if not all, human solid tumors (1, 3). However, the molecular mechanisms underlying tumoral MHC-I expression downregulation remain largely unknown.

The reduction or loss of MHC-I expression in cancers can occur not only through genomic mutations but also through non-genomic mechanisms that leverage epigenetic and transcriptional silencing of the MHC locus and/or antigen-processing machinery. Multiple regulators such as NOD-like receptor (NLR) family, caspase recruitment domain-containing 5 (NLRC5), NF- κ B and IFN regulatory factor 1 (IRF-1) promote MHC-I genes exposure to cytokines such as TNF- α and IFN- γ (5). The Enhancer of Zeste Homolog 2 (EZH2), a catalytic component of Polycomb Repressive Complex 2 (PRC2) which in turn is involved in regulating chromatin organization (6), has been identified as a potential therapeutic target for multiple cancers due to its frequent overexpression and role in tumor progression (7). Recent studies have shown that EZH2 contributes to tumor immune evasion by trimethylation of lysine 27 of histone H3 (H3K27me3) on the *B2m*

promoter in cancer cells (8). Indeed, EZH2 is found to be overexpressed in various cancers with poor neoantigen presentation (8).

In this study, we identified *USP22*, an oncogene involved in promoting cancer cell growth and tumor immune evasion (9), as a negative regulator of MHC-I expression across a variety of human and mouse cancer cell lines. Targeted CRISPR mediated deletion of *Usp22* resulted in enhanced tumor cell antigen presentation and tumor-specific CD8⁺ cell immunity. At the molecular level, USP22 associates with and deubiquitinates EZH2, thereby protecting it from proteasomal degradation. Analysis of human cancer tissues revealed a positive correlation of USP22 with EZH2, both of which were negatively correlated with MHC-I expression and intratumoral CD8 T cell infiltration. Importantly, increased USP22 expression is associated with ICB immunotherapeutic resistance and pharmacological USP22 inhibition overcomes ICB resistance.

Results

USP22 is a negative regulator of MHC-I mediated neoantigen presentation in tumor cells.

We and others have recently revealed that inhibition of USP22 plays a role in both onco-targeting and boosting the anti-tumor immune response (9, 10). To further explore the role of tumoral USP22 in evading immune surveillance, we analyzed the potential effect of Usp22 inhibition on neoantigen presentation. CRISPR-mediated deletion of *Usp22* in mouse prostate cancer RM1, colon cancer MC38, and breast cancer 4T1 cells resulted in a substantial elevation in the expression of both H-2Kb/d and β2M, two subunits of the MHC-I complex (Fig. 1A and S1A). Flow cytometry analysis further confirmed the increase in cell surface expression of H-2Kb/d and β2M in Usp22-null tumor cells (Fig. 1B). Usp22 inhibition resulted in a similar increase in HLA-ABC and β2M expression in both human prostate cancer PC3 and triple negative breast cancer MDA-MB-231 cells (Fig. 1A). Further real-time RT-PCR analysis detected an elevation of H2D1 (encode H-2Kb) and B2m (encode $\beta 2M$) mRNA levels by Usp22 ablation (Fig. 1C and S1B). Consistently, pharmacological USP22 inhibition by USP22i-S02, a small-molecule inhibitor developed by our group (11), boosted both H-2Kb and β2M expression (Fig. S1C). Conversely, Usp22 over-expression resulted in a modest but statistically significant decrease in MHC-I expression (Fig. S1D). In addition, MHC-II was undetectable in RM1 cells, and only very low levels were observed in MC38 cells. In both cell lines, neither *Usp22* knockout nor overexpression altered MHC-II expression (Fig. S1E). It is well-established that IFN- γ is a critical inducer for MHC-I expression (12). To investigate the role of USP22 in IFN-γ-induced tumoral MHC-I expression, we analyzed its effects under these conditions. As expected, IFN- γ treatment substantially increased the expression of β2M and H2Kb/d in WT cancer cells. However, in *Usp22* knockout tumor cells, IFN-γ treatment failed to further enhance MHC-I expression (Fig. S1F-H). These results indicate that USP22 is a negative regulator of MHC-I expression possibly at the transcriptional level, implying that USP22 achieves its tumor immune evasive functions through, at least in part, suppression of MHC-I expression.

MHC I-mediated antigen presentation is crucial for activating CD8⁺ T cells (3). To determine the impact of USP22-mediated MHC-I downregulation on CD8⁺ T cell immunity, we generated WT and Usp22-deficient RM1 and MC38 cells stably expressing OVA (13-15). As expected, Usp22 ablation cells exhibited a higher level of the OVA peptide (SIINFEKL)-bound MHC-I complex (pMHC-I) (Fig. 1D and S1I). Reconstitution with Usp22, but not the catalytically inactive Usp22 (Usp22 C185A) mutant, in Usp22-deficient cells completely reversed the increased MHC-I levels (Fig. S1J), suggesting that the deubiquitylase activity of USP22 is required in downregulating MHC-I-mediated antigen presentation. Co-culture of CD8⁺ OT-I T cells with either Usp22 KO MC38 or RM1 cancer cells with stable OVA expression enhanced CD8⁺ T cell activation, indicated by elevated CD69 expression, and tumor cell killing (Fig 1E-H). Furthermore, intracellular staining confirmed the increased production of granzyme B, IFN- γ , and TNF- α by CD8⁺ OT-I T cells (Fig. 1G & H). Consistent with these findings, pharmacological inhibition of Usp22 in tumor cells by treatment with USP22i-S02 enhanced the activation of CD8⁺ OT-I T cells. (Fig. 1I & J and S1K). Moreover, ELISA analysis detected a substantial increase in both IFN-γ and TNF-α secretion in the supernatant when CD8⁺ OT-I T cells were cocultured with Usp22 KO or pharmacological inhibition tumor cells (Fig. 1K & L). Collectively, these results indicate that USP22 downregulates MHC-I to suppress CD8+ T cell anti-tumor immunity. To support this conclusion, targeted deletion of B2m, an essential component of MHC-I, while having no effect on cell proliferation (Fig. 1M and Fig. S2A & B) as reported (16), totally abolished the increased CD8⁺ OT-I T cellmediated killing of Usp22-deficient tumor cells (Fig. 1N), as well as the activation and increased secretion of IFN- γ and TNF- α (Fig. 10-Q, and S2C-F). These results indicate that tumoral *Usp22* inhibition-mediated increase in CD8⁺T cell antitumor immunity is dependent on MHC-I upregulation.

Tumoral *Usp22* inhibition enhances anti-tumor immune response through upregulating MHC-I-mediated neoantigen presentation to CD8 T cells.

Next, we investigated the functional consequences of *Usp22*-mediated MHC-I downregulation in the antitumor immune response. Importantly, CRISPR deletion of *Usp22* led to a nearly complete rejection of syngeneic RM1 prostate cancer in immunocompetent C57BL/6 mice (Fig. 2A & B). In contrast, *Usp22* suppression only resulted in a modest reduction in RM1 tumor growth both in RAG1 KO mice (Fig. 2C & D), as well as *in vitro* (Fig. S3A). These results support our previous conclusion that while *Usp22* is an oncogene and promotes tumor growth (17-20), the antitumor immune response plays a much greater role in tumor rejection. To support this hypothesis, we confirmed the increase in MHC-I expression in *Usp22*-null tumors (Fig. 2E), along with a marked increase in intratumoral CD8 T cell infiltration as analyzed by both flow cytometry (Fig. 2F) and IHC staining (Fig. 2G). Intracellular staining detected a marked increase in CD8 T cell production of granzyme B, IFN-γ and TNF-α (Fig. 2H-J). Therefore, tumoral *Usp22* inhibition enhances CD8 T cell antitumor immunity. To support this, further depletion of CD8 T cells using CD8-depleting antibody (αCD8) largely diminished the increased rejection of *Usp22* deficient tumors (Fig. 2K & L).

In addition to RM1 prostate cancer, we confirmed that *Usp22* inhibition impeded the growth of both orthotopic 4T1 triple negative breast cancer (Fig. S3B & C) and MC38 syngeneic tumors (Fig. S4A & B). Additionally, the tumor suppressive efficacy of *Usp22* inhibition was modest when MC38 tumor cells were implanted into RAG1 KO mice (Fig. S4C & D). The increased tumor suppression by *Usp22* deletion is associated with increased tumor cell surface H-2Kb and β2m expression (Fig. S3D & S4E), the elevated tumoral-infiltrating CD8 T cells (Fig. S3E & F, S4F & G) and their production granzyme B, interferon-γ (IFN-γ), and TNF-α (Fig. S3G-I, S4H-J). Further depletion of CD8 T cells using CD8-depleting antibody (αCD8) largely diminished the increased regression of *Usp22* deficient tumors (Fig. S3J & K, S4K & L). These results indicate that *Usp22* promotes the evasion of CD8 T cell antitumor immunity across a broad spectrum of cancer types through, at least in part, downregulating MHC-I expression. To further support this conclusion,

we found that silencing of *B2m* expression completely abolished the improved antitumor immune response associated with *Usp22* inhibition (Fig. 2M-P and S4M-P).

Further, we observed that *Usp22* targeted inhibition synergized with anti-PD-1 treatment leading to a complete rejection of orthotopic 4T1 triple negative breast cancer, MC38 colon cancer and RM1 prostate cancer (Fig. S5A-F). Flow cytometry analysis of intra-tumoral immune cells confirmed the synergistic effects of tumoral *Usp22* inhibition in boosting antitumor immunity with increased CD8 T cell infiltration and production of granzyme B and IFN-γ (Fig. S5G-I). Similar to the CRISPR targeted *Usp22* inhibition, USP22i-S02 treatment synergized with anti-PD-1 resulted in a nearly complete inhibition of both RM1 and MC38 tumor growth with increased CD8 antitumor immunity (Fig. S6). These results indicate that tumoral *Usp22* inhibition sensitizes ICB antitumor immunotherapy.

Usp22 inhibits MCH-I expression through upregulating EZH2 in cancer cells.

As a ubiquitin-specific peptidase, *Usp22* often achieves pathological functions through protecting its substrates from ubiquitination-mediated protein degradation (11, 21, 22). We then analyzed the protein expression levels of previously identified MHC-I regulators, including PRC2 proteins (EZH1, EZH2, SUZ12 & EED) (8), NLRC5 (23), and METTL3 (24) and METTL14 (25), in *Usp22*-null versus control cells to identify potential substrates of USP22. Interestingly, among these MHC-I regulators, *Usp22* depletion resulted in a distinct reduction in the protein expression of EZH2, a core component of the PRC2 complex. In contrast, the expression of other PCR2 complex proteins including EED, EZH1 and SUZ12 were unaffected (Fig. 3A). As a methyltransferase, EZH2 has been shown to methylate histone H3 lysine 27 (H3K27me3) which is critical for tumorigenesis in part through the silencing of MHC-I gene transcription (26, 27). Along with EZH2 downregulation, the trimethylation level of histone H3 lysine 27 in *Usp22* null tumor cells was reduced (Fig.

3A). In contrast, *Usp22* depletion did not alter the expression of NLRC5, METTL3 and METTL14 (Fig. S7A). Similar to that of *Usp22* targeted deletion, treatment of tumor cells with USP22i-S02 led to a substantial reduction in EZH2, but not EED, EZH1 and SUZ12 (Fig. 3B). Furthermore, IHC staining confirmed the reduced EZH2 expression in *Usp22*-null tumor cells (Fig. 3C and Fig. S7B). Intriguingly, neither genetic nor pharmacological *Usp22* inhibition had any effect on *EZH2* mRNA expression in MC38, 4T1 and RM1 tumor cells (Fig. S7C), suggesting that *Usp22* regulates EZH2 at the post-transcriptional level. Indeed, treatment with the proteasomal inhibitor MG132, but not the lysosomal inhibitor chloroquine, fully rescued EZH2 protein expression in cancer cells either with *Usp22* deletion or treated with the USP22 small-molecule inhibitor S02 (Fig. 3D, Fig. S7D). These results suggest that USP22 suppresses tumoral MHC-I expression through EZH2 upregulation at the post-transcriptional level.

EZH2 is known to silence MHC-I expression through epigenetic suppression (28, 29). Indeed, both the recruitment of EZH2 to the promoter regions of *B2m* and *H2Kb* and their H3K27me3 modification levels, was decreased in USP22-null tumor cells (Fig. 3E & F). Consistently, both genetic or pharmacologic inhibition of EZH2 enhanced H-2Kb and β2M expression (Fig. S7E-H) and reduced H3K27me3 modification levels on *H2K1* and *B2m* promoter region in RM1 and MC38 cancer cells (Fig. S7I). In contrast, the recruitment of KDM6A, a histone-demethylase known to regulate MCH-I expression through inhibiting H3K27me3 at *B2m* and *H2Kb* promoter regions, was unaltered by USP22 inhibition (Fig. S7J). Collectively, our results indicate that USP22 represses antitumor immunity in part through potentiating EZH2-mediated transcriptional downregulation of MHC-I expression.

USP22 is a de novo EZH2-specific deubiquitinase.

To further delineate underlying molecular mechanisms by which USP22 specifically controls EZH2

protein expression in tumor cells, we first determined whether USP22 interacts with EZH2. Indeed, western blotting detected USP22 protein in the anti-EZH2 immunoprecipitated from the lysates of RM1 and MC38 cells (Fig. 3G). Reciprocally, EZH2 was detected in the anti-USP22 pulldown (Fig. 3G). The interaction between USP22 and EZH2 was further confirmed in HEK-293T cells transfected with Myc-tagged USP22 and Flag-tagged EZH2 (Fig. 3H). Additionally, EZH2 protein was detected from GST-USP22 pulldown but not GST protein alone (Fig. 3I). USP22 protein consists of an N-terminal zinc finger domain followed by a C19 ubiquitin-specific peptidase domain. We then generated USP22 truncated mutants and found that the C-terminus C19 peptidase domain, but not the N-terminal zinc finger-containing region, is sufficient to mediate USP22 interaction with EZH2 (Fig. 3J & K). Consistent with this, mutation of the critical cystines in the zinc finger structure, did not affect USP22 interaction with EZH2 (Fig. 3L). Molecular docking analysis revealed that the USP22 C-terminal U19 domain mediates its interaction with EZH2 (Fig. 3M). Collectively, these results indicate that USP22 is a de novo interacting partner of EZH2 in tumor cells.

A deubiquitinase often inhibits the ubiquitination of its interacting proteins (30). Indeed, ectopic expression of *Usp22* inhibited the ubiquitination of EZH2 (Fig. 3N). In contrast, the catalytically inactive *Usp22*-C185A while still interacting with EZH2, did not show any effect on EZH2 ubiquitination (Fig. 3L & N). Conversely, targeted deletion of *Usp22* resulted in enhanced EZH2 ubiquitination both RM1 and MC38 tumor cells (Fig. 3O). Collectively, our results indicate that USP22 is a *de novo* deubiquitinase of the MHC-I suppresser EZH2 in cancer cells.

EZH2 is responsible for USP22-mediated downregulation of MHC-I.

A deubiquitinase suppresses the ubiquitination of its target proteins to regulate their biological functions through degradation or subcellular distribution. Our results that targeted *Usp22* inhibition decreased EZH2 protein but not its mRNA expression levels (Fig. 3A-C and Fig. S7C), indicate that USP22 upregulates EZH2

through suppressing its ubiquitination-mediated protein degradation. As expected, overexpression of wildtype *Usp22*, but not *Usp22*-C185A, improved EZH2 stability (Fig. 3P). In contrast, *Usp22* deletion promoted EZH2 protein degradation, which was fully rescued by wildtype *Usp22*, but not *Usp22*-C185A (Fig. 3Q & R).

Unexpectedly, we observed that IFN-γ treatment led to a distinct reduction in USP22 protein levels (Fig. S1E). Consequently, a marked decrease in EZH2 protein was also detected in tumor cells following IFN-γ treatment. Notably, IFN-γ treatment did not affect *Usp22* or *Ezh2* mRNA levels (Fig. S8A), suggesting that IFN-γ regulates USP22 and its substrate EZH2 at a posttranslational level. Supporting this, treatment with the proteasome inhibitor MG132 fully protected USP22 protein from IFN-γ-induced downregulation, whereas the lysosomal inhibitor chloroquine failed to rescue USP22 and EZH2 expression (Fig. S8B). Further analysis revealed that IFN-γ treatment promotes USP22 ubiquitination and degradation (Fig. 4B & C). Interestingly, IFN-γ also disrupted the interaction between USP22 and EZH2 after treatment with IFN-γ for only 15 minutes even before USP22 and EZH2 degraded (Fig. 4D). These findings suggest that IFN-γ induces MHC-I expression by promoting USP22 ubiquitination-mediated degradation. Consistent with this, genetic inhibition of IFN-γ receptor 1 (*IFNGR1*) completely abolished IFN-γ-induced USP22 downregulation (Fig. S8C).

Our data thus far demonstrate that USP22 protects EZH2, a known negative regulator of MHC-I expression (8), from ubiquitination-mediated proteasomal degradation, suggesting that USP22 promotes tumor evasion of CD8 T cell antitumor immunity through potentiating EZH2-mediated MHC-I downregulation. Indeed, reconstitution of *Ezh2*, but not its inactive methyltransferase mutant either by F667I mutation, or by deletion of the catalytic SET domain, fully reversed MHC-I expression levels in *Usp22*-null tumor cells (Fig. S8D-F). Consistent with our data that USP22 represses MHC-I expression through EZH2-mediated H3K27me3 at *B2m* and *H2Kb* promoters (Fig. 3F), further real-time-PCR analysis confirmed that that the USP22-EZH2 axis controls MHC-I expression at the mRNA level (Fig. S8G). Consistently, isolated RM1 and MC38 cells with lower β2M and pMHC-I levels exhibited higher levels of USP22 and EZH2 protein, and *vice*

versa (Fig. 4E & F). In contrast, neither USP27 nor EZH1 expression was associated with β2M or pMHC-I levels (Fig. 4E & F). Therefore, when co-cultured with OT-I CD8 T cells, expression of EZH2, but not its catalytically inactive mutants in *Usp22*-null tumor cells, totally diminished the increase in OT-I CD8 T cell activation including the production of granzyme B, IFN-γ and TNF-α, cell surface expression of CD69 as well as OT-I mediated cytotoxicity (Fig. 4G & H and Fig. S8H & I). Conversely, further analysis of surviving tumor cells 48 hours after co-cultivation with OT-I CD8 T cells showed a higher USP22 and EZH2, but not EZH1 and USP27 expression (Fig. 4I), implying that the increased USP22 and EZH2 expression is involved in tumor immune evasion.

Consistent with our *in vitro* studies, stable reconstitution of Ezh2, but not Ezh2 F667I or Δ SET mutant, largely abrogated the tumor-suppressive effects by the targeted Usp22 inhibition (Fig. 4J & K and Fig. S9A & B). Cell surface staining of MHC-I expression on tumor cells indicated that overexpression of Ezh2, but not Ezh2 F667I or Δ SET mutant, in Usp22-null cells impaired MHC-I expression (Fig. 4L and Fig. S9C). Consequently, the increased CD8⁺ T cell infiltration as well as GZMB production, were largely reversed by the reconstitution of Ezh2, but not its Ezh2 F667I or Δ SET mutants (Fig. 4 M & N and Fig. S9 D & E). Thus, USP22 drives immune evasion largely in an EZH2-dependent manner.

Clinical relevance of USP22-EZH2-β2M signaling in tumorigenesis.

We next determined whether the USP22-EZH2-β2M pathway was associated with CD8 T cell infiltration into tumors. A human breast cancer tissue microarray was used for multiplex immunofluorescence staining as reported (31). Consistent with our findings that USP22 protects EZH2 from ubiquitination-mediated degradation, both USP22 and EZH2 proteins were highly expressed and positively correlated in tumor tissues compared with adjacent normal tissues (Fig. 5A & B and S10A & B). Importantly, a substantial lower β2M expression levels, along with a markedly reduced intra-tumoral CD8⁺ T cell infiltration was detected in USP22

high vs low tumor groups (Fig. 5A & C). Therefore, a negative correlation of tumoral USP22 with tumoral β2M, and with CD8⁺ T cell infiltration was detected (Fig. 5B). These results support our conclusion that high USP22 expression contributes to tumor immune evasion through potentiating EZH2-mediated HLA-I downregulation.

Consistent with our observations in human breast cancers, immunohistochemical staining of EZH2, USP22, β2M, and CD8* in serial tissue sections in human prostate and colon cancer tissue microarrays confirmed the increased expression of USP22 and EZH2 in tumors vs benign tissues (Fig. 5D-G and S11-12A & B). Both β2M and CD8 intra-tumoral infiltration were markedly lower in the USP22 high vs USP22 low tumors (Fig. 5D-G). We further unbiasedly analyzed the *USP22* and *B2M* transcripts in breast cancer cell lines listed in Cancer Cell Line Encyclopedia (CCLE). The results demonstrated an inverse correlation between *USP22* and *B2M* expression (Fig. 5H). TCGA analysis showed a similar negative association of USP22 expression with CD8 scores in breast, prostate and lung cancer (Fig. 5I). Collectively, these results indicate that the USP22-EZH2-β2M pathway is a common molecular mechanism for poor MHC-I expression in a broad spectrum of human cancers.

Elevated USP22 expression is linked to poor ICB response.

Poor neoantigen presentation, either due to low mutational load or reduced HLA-I expression, or both, is a critical driver of ICB resistance (1, 3). Our discovery that USP22 mediated MHC-I/HLA-I downregulation prompted us to evaluate the association of USP22 expression levels with ICB resistance. We collected lung biopsies from a cohort of 32 patients diagnosed with non-small cell lung cancer (NSCLC) prior to ICB immunotherapy with α PD-1 (sintilima, tislelizumab, or camrelizumab, all of these have been approved by China national medical products administration for NSCLC treatment). After an up to 30-month following up of clinical immunotherapeutic studies, we confirmed that out of these 32 patients, 22 were clinically classified as non-responders who were resistant to the α PD-1 ICB therapy and 10 were responders (Supplement table

1). The responders showed prolonged progression-free survival (PFS) relative to non-responders (Fig. 6B). Importantly, we found that high pretreatment expression of USP22 was predictive of ICB resistance (Fig. 6C). As expected, a higher frequency of intra-tumoral CD8 T cell infiltration and high tumor MHC-I expression was detected in responders compared with non-responders (Fig. 6A & D and S13A). Tumor tissues from ICB non-responders exhibited higher levels of both tumoral USP22 and EZH2 expression, and lower tumoral β2M expression when compared to biopsies from ICB responsive patients (Fig. 6A & D). These results suggest that elevated USP22 expression is a potential biomarker to predict ICB responsiveness in lung cancer. To further support this notion, USP22/EZH2/β2M levels and CD8 T cell infiltration were associated with notable differences in PFS following ICB therapy regardless of ICB responsiveness (Fig. 6E and S13B-D).

In addition, consistent with our findings in breast, prostate and colon cancers (Fig. 5 and S10-12), tumoral USP22 and EZH2 protein expressions exhibited a strong positive correlation, and both were inversely correlated with tumoral β2M expression and with CD8* T lymphocytes infiltration in lung cancer (Fig. 6F & G). We next explored the diagnostic significance of *USP22* expression in ICB responsiveness through unbiased analysis of RNA-seq data from a phase-II I-SPY2 trial, using durvalumab, olaparib and neoadjuvant paclitaxel in patients with triple negative breast cancer (32). The average levels of *USP22* transcripts were higher in non-responders relative to responders (Fig. 6H), which were inversely associated with levels of *B2M* transcripts (Fig. 6H). Consistently, another RNA-seq dataset from patients with advanced melanoma treated with ipilimumab followed by nivolumab (33) revealed an increase in *USP22* transcripts in non-responders compared to responders (Fig. 6I), which were inversely correlated with *B2M* transcript levels (Fig. 6I). These results further support our conclusion that increased USP22 is associated with ICB therapy resistance.

Targeting USP22 overcomes ICB resistance.

We then established a preclinical orthotopic triple negative breast cancer 4T1 syngeneic model that is

fully resistant to αPD-1 immunotherapy to test whether USP22-mediated MHC-I suppression is responsible for ICB resistance. Briefly, mice with pre-established orthotopic 4T1 TNBCs were treated with α PD-1 antibody when the tumor volume reached approximately 50-100 mm³. At day 18 post-tumor inoculation, tumors were harvested, CD45⁻ tumor cells were isolated and cultured for 2-3 passages in vitro, denoted as 4T1 cycle 1 (C1) (Fig. S14A). 4T1-C1 cells were then re-implanted followed by the same α PD-1 treatment regime. Following three sequential cycles (4T1-C3), the tumors exhibited complete resistance to αPD-1 treatment (Fig. S14A, Fig. 7A & B). We then named the α PD-1 resistant 4T1 tumor cells as 4T1R. Flow cytometry and western blotting analysis of 4T1R cells detected a substantial reduction in MHC-I expression levels, with increased USP22 and EZH2 protein expression (Fig. S14B & C). In contrast, the surface expression of checkpoint molecules PD-L1, CD73 and CD155 on 4T1R cells were slightly increased when compared to parent 4T1 cells (Fig. S14B). Further RT-PCR analysis detected a remarkable reduction in several key genes involved in antigen processing and presentation, including B2m, H2D1, Tap1, Tap2, and Psmb9 in 4T1R cells (Fig. S14D). A remarkable increase in the mRNA expression of *Usp22* and *Ezh2* was detected in 4T1R cells compared to 4T1 cells (Fig. S14D). Consistent with the in vitro 4T1R characterization results, analysis of CD45 cells from orthotopic 4T1R tumors relative to 4T1 tumors found decreased expression of MHC-I (Fig. S14E). Unexpectedly, cell surface PD-L1 levels were comparable between 4T1 and 4T1R cells (Fig. S14F). These results indicate that the increased USP22 expression, which reduces MHC-I, rather than the altered PD-L1 expression, is largely responsible for anti-PD-1 ICB therapeutic resistance.

Flow cytometric analysis of tumoral infiltrating lymphocytes revealed a reduced proportion of CD8⁺ T cells and decreased production of GZMB and IFN-γ in 4T1R tumors (Fig. S14G). We also noticed that 4T1R tumors showed increased frequencies of total CD4⁺ T cells and regulatory T cells (Tregs, CD4⁺CD25⁺FoxP3⁺), as well as a slight, but not statistically significant, increase of myeloid-derived suppressor cells (MDSCs, CD11b⁺Ly6G⁺) compared with 4T1 tumors (Fig. S14G). Additionally, we didn't observe any changes in the

frequency of natural killer cells (CD3⁻NK1.1⁺) (Fig. S14G). Therefore, these results indicate that USP22 represses MHC-I expression to architect an immune suppressive tumor microenvironment with increased Tregs and MDSCs and decreased CD8 T cells promoting ICB resistance.

We then asked whether *Usp22* inhibition is sufficient to overcome ICB resistance. Indeed, targeted *Usp22* ablation inhibited the growth of both 4T1R and 4T1 orthotopic tumors (Fig. 7C & D), suggesting that elevated *Usp22* expression is largely responsible to ICB resistance. Flow cytometry analysis of cell surface level of MHC-I on 4T1R USP22-null and control tumors showed that *Usp22* deficiency in 4T1R tumors led to increased MHC-I expression relative to 4T1 control tumors level (Fig. S14H). Consistently, *Usp22*-null 4T1R tumors exhibited a greater frequency of CD8⁺ T cells infiltration as well as a higher proportion of GZMB and IFN-γ producing CD8⁺ T cells (Fig. S14I).

Consistent with our results from targeted *Usp22* genetic deletion, treatment of mice with preestablished orthotopic 4T1R tumors by USP22i-S02 inhibited tumor growth (Fig. 7E & F). In contrast to our
earlier finding that 4T1R is resistant to αPD-1, combined treatment with USP22i-S02 and αPD-1 further
inhibited 4T1R tumor growth (Fig. 7E & F). Flow cytometry analysis revealed that USP22i-S02 treatment
enhanced MHC-I, but not PD-L1 expression (Fig. 7G-I). In contrast, administration αPD-1 alone didn't
influence cell surface MHC-I or PD-L1 expression (Fig. 7G-I). Supporting our previous findings that USP22
acts as a Foxp3 stabilizer through deubiquitinating Foxp3 (9, 11), we found a reduction of Foxp3 mean
fluorescence intensity as well as reduced percentages of intratumoral Foxp3* Treg cells upon administration
of USP22i-S02 (Fig. 7J & K). Consequently, USP22i-S02 in combination with anti-PD1 induced a greater
frequency of CD8* T cells compared with mice treated with either USP22i-S02 or anti-PD1 alone (Fig. 7L).
We also observed that either USP22i-S02 alone or in combination with anti-PD1 contributed to enhanced
proportions of GZMB and IFN-γ producing CD8* T cells (Fig. 7M & N). In contrast, αPD-1 administration did
not influence CD8* T cells infiltration and function (Fig. 7L-N). Consistent with 4T1 R model, inhibition of

Usp22 in LLC1 cells, a well-established syngeneic tumor model that is resistant to ICB (34), inhibited tumor growth (Fig. S15A-B). Usp22 inhibition combined with anti-PD1 induced a greater tumor regression and resulted in a higher percentage of CD8⁺ T cells infiltration compared with mice treated with anti-PD1 alone (Fig. S15A-C). Collectively, our findings reveal the USP22-EZH2-MHC-I axis driving tumor immune evasion. The upregulation of USP22, coupled with its inverse correlation with HLA-I expression and CD8⁺ T cell infiltration, positioning USP22 as a potential biomarker for predicting resistance to ICB therapy. Furthermore, pharmacological inhibition of USP22 offers a promising strategy to overcome ICB resistance, providing a therapeutic avenue for the treatment of a wide range of human solid tumors (Fig. 7O).

Discussion

The current study has identified USP22 as a critical regulator responsible for poor MHC-I expression through potentiating EZH2-mediated epigenetic silencing. Furthermore, USP22 inhibition holds great potential to overcome the current limitations with immune checkpoint blockade therapy. This conclusion is supported by the following discoveries: first, immunostaining revealed a strong positive correlation between expression of USP22 and β2M in multiple types of human solid tumors including breast, colon, prostate and lung cancers; second, both genetic and pharmacological USP22 inhibition increased MHC-I and HLA-I expression in mouse and human cancer cells, respectively; third, USP22 represses MHC-I expression through EZH2-mediated transcriptional silencing; fourth, EZH2 is a bona fide substrate of USP22 in human and mouse tumor cells; fifth, increased USP22 positively correlates with EZH2, but negatively correlates with HLA-I, in human tumors, which predicts ICB response in lung adenocarcinoma patients; and finally, USP22 inhibition overcomes anti-PD1 resistance in the treatment of orthotropic triple negative breast cancer.

Tumor cells escape antitumor immune surveillance through inhibiting neoantigen presentation, such as downregulating the expression and function of MHC-I molecules, which are crucial for presenting antigens to cytotoxic CD8+ T cells (5). Direct mutations in the genes involved in the MHC-I or HLA-I pathway, such as β2M mutation, which can lead to reduced expression or absence of these molecules, has been identified in some cancer patients (35). Studies have implicated epigenetic and transcriptional silencing of MHC-I expression, such as through increased histone methylation mediated by proteins like EZH2, in the development and progression of many types of human cancers. Similarly, the EZH2-containing PRC2 transcriptional co-suppressive complex and other regulatory proteins keep chromatin in a transcriptionally inactive state, reducing the expression of MHC-I and antigen-processing components (8). Our study here identifies USP22 as a critical MHC-I repressor by protecting EZH2-mediated transcriptional inhibition of MHC-I transcription. At the molecular level, USP22 functions as an EZH2-specific deubiquitinase to protect EZH2

from ubiquitin-mediated proteasomal degradation. To support this conclusion, our immunostaining analysis detected a positive correlation between USP22 and EZH2, which were both negatively associated with tumoral β2M expression and CD8 T cell infiltration in human breast, colon, prostate and lung cancers. Interestingly, USP22 appears to selectively control EZH2, but not any other PCR2 complex proteins including EZH1, SUZ12 and EED in tumor cells. Therefore, our study defines USP22 as a EZH2-specific deubiquitinase to potentiate the epigenetic silencing of MHC-I gene expression. Constant with our study, a comprehensive genome-wide profiling of the immune-evasive molecular signature of USP22 also identified USP22 as a negative regulator for downregulation of MHC-I in pancreatic tumor cells (36). Importantly, this elegant study also discovered the transcriptional suppressive function of EZH2 complex is regulated by USP22. Our discovery that EZH2 is a bona fide substrate provides a direct connection between USP22 and EZH2 in silencing tumoral MHC-I silencing. In addition, a recent genome-wide CRISPR screening also identified USP22 as a hit in regulating MHC-I expression (37). Therefore, USP22-mediated MHC-I suppression appears to be a critical mechanism underlying tumor evasion of CD8 T cell immunity in a verity of human cell types. In addition to USP22, the ubiquitin-like modifier activating enzyme 1 (UBA1) has been shown to downregulate MHC-I expression for tumor immune evasion (38). Moreover, several ubiquitin regulators including the epigenetic regulator ubiquitin-like with PHD and ring finger domains 1 (UHRF1) (39), RNF185 (40), and USP8 (41) regulate tumoral MHC-I expression. On the other hand, the ubiquitin-like protein 3 (UBL3) corporates with the E3 ligase MARCH to target MHC-II for ubiquitination (42). It will be interesting to further delineate whether, and if yes, how different ubiquitin pathways corporately control tumor neoantigen presentation through either MHC-I down-regulation or neoantigen processing, or both, during immune evasion. In addition to MHC-I, it has been recently reported that EZH2 inhibition stabilizes PD-L1 expression through USP22-mediated deubiquitination is intriguing (43). Our study demonstrates that USP22 stabilizes EZH2, suggesting a potential feedback loop between USP22 and EZH2 in the regulation of PD-L1 expression

and possibly also MHC-I. Moreover, the role of EZH2 in PD-L1 regulation appears to be context-dependent. For instance, EZH2 has been reported to negatively regulate PD-L1 expression in hepatocellular carcinoma (44), while other studies have shown that shRNA-mediated EZH2 knockdown suppresses both mRNA and protein levels of PD-L1 L1 (45). These observations highlight the complexity of the regulatory network and underscore the need for further investigation into the roles of USP22 and EZH2 in modulating PD-L1 expression across different cancer types.

Cancer immunotherapy has indeed transformed the standard of care for many advanced cancers. However, clinical outcomes of cancer immunotherapy are still limited for most solid tumors. For example, the current checkpoint blockade immune therapy has so far proved disappointing in the treatment of colorectal cancers, patient population (46). While CRCs have been classified as "cold tumors", often characterized by low or absent PD-L1 expression, clinical findings indicate that approximately 60% of human CRCs exhibit PD-L1 positivity (47). Thus, the lack of PD-L1 expression does not seem to be the primary factor driving CRCs' "cold tumor" status. In the case of patients with aggressive triple-negative breast cancer, anti-PD1 immune checkpoint inhibitors (such as pembrolizumab), when combined with chemotherapy, are now part of standard care for high-risk stage II/III and advanced PD-L1⁺ TNBC (48). The pathologic complete response (pCR) rate is 62% in patients with a PD-L1 combined positive score (CPS) ≥1 and 50% in those with a PD-L1 CPS<1 (49). Yet a substantial proportion (up to 40% of PD-L1⁺ and 50% of PD-L1^{low/-}) of TNBCs are classified as "cold tumors". Therefore, PD-L1 expression does not seem to be the primary determinant of "cold tumor" status for both CRCs and TNBC. Indeed, the ICB resistant 4T-1R TNBC cells show slightly higher PD-L1 and CD73 expression levels, both of which are USP22 targets (31, 50). Therefore, the reduced MHC-I expression due to increased USP22 appears to be the major driver of anti-PD-1 resistance. Importantly, we observe that all anti-PD-1 responding lung cancer patients show statistically significant lower USP22 expression levels, which are reversibly associated with increased tumoral HLA-I (β2M) expression and CD8

T cell infiltration. Therefore, our results suggest that USP22 expression levels alone or combined with HLA-I expression levels and CD8 T cell infiltration frequency prior to ICB, could serve as a more accurate biomarker to predict the ICB immunotherapeutic response for lung cancer treatment. Cancer patients can exhibit either primary resistance (lack of initial response) or acquired resistance (loss of response after an initial benefit). Of note, the patients with heterogenous USP22 expression tumor (mixed with high and low expression) exhibit an initial responsiveness to ICB immunotherapy and ultimately develop acquired resistance to the treatment. While our data demonstrates a strong negative correlation between USP22 and β2M across multiple human cancer types, we were only able to recruit 32 lung cancer patients to assess the predictive value of USP22 expression for anti-PD-1 immune checkpoint blockade (ICB) responsiveness. Future studies with larger cohorts and across additional cancer types will be necessary to establish USP22 expression as a reliable biomarker for predicting ICB therapy responsiveness.

Recent studies reveal two main factors that contribute to resistance to ICB therapy in cancer treatment:

(i) an immunosuppressive TME due to increased infiltration of Tregs (51-53), myeloid-derived suppressor cells and immune suppressive macrophages (54); and (ii) impaired tumor antigen presentation due to relatively low mutational burden and reduced MHC-I expression (55). Hence, targeting immunosuppressive TME and enhancing neoantigen presentation are essential strategies to improve the efficacy of immunotherapy for treatment of tumors including TNBC and lung cancer. Importantly, our discovery here that tumoral USP22 inhibition increases MHC-I expression, together with our recent works that USP22 deletion diminishes pro-tumor Treg suppressive activity (9, 11), indicate that USP22 plays a critical role in immunotherapeutic resistance. Furthermore, in cancer cells, USP22 promotes expression of PD-L1 and CD73 (31, 50), two checkpoint receptors responsible for tumor immune evasion. In addition to its immune evasive functions, elevated expression of USP22 correlates with poor prognosis in a variety of human tumors (56, 57) and functions as an oncogene by targeting cyclins, c-Myc, and p53, to inhibit apoptosis and promote

cell cycle progression (17, 58-62). USP22 also promotes chemotherapy resistance by inhibiting Baxmediated apoptosis (63) and is reportedly a critical cancer stem cell gene (64). Indeed, we have previously demonstrated that USP22 is required to maintain TNBC stemness and that pharmacological USP22 inhibition reduces mouse 4T1 and human TNBC PDX metastasis to the lungs (20). These discoveries indicate that targeting USP22 enhances both immune boosting and onco-targeting dual efficacy in antitumor treatment and holds great potential to overcome the current limitations with ICB resistance. Indeed, our study here demonstrated that both genetic and pharmacological USP22 suppression improved the anti-PD-1 therapeutic activity in treatment of the orthotopic 4T1 triple negative breast cancers that are completely resistant to anti-PD-1, providing a strong rationale for USP22 targeting to overcome the ICB therapy resistance. This superior therapeutic efficacy of USP22 inhibition is in part through enhancing MHC-I-mediated CD8 cytotoxic activity. In addition to CD8 T cells, MHC-I is a known suppressor of NK cell activation. The increase in MHC-I expression following USP22 inhibition may potentially reduce NK cell-mediated tumor killing. Interestingly, research from the Stanger lab (36) demonstrated that loss of USP22 in pancreatic ductal adenocarcinoma led to enhanced NK cell infiltration, suggesting that additional mechanisms may influence the impact of USP22 targeting on NK cell immunity, which deserve extensive future studies to explore the underlying cellular and molecular mechanisms. Our group is currently evaluating the preclinical efficacy of the first USP22-specific small molecule inhibitor in overcoming the ICB immunotherapeutic resistance for the treatment of a broad spectrum of solid tumors and conducting IND enabling studies to translate USP22 specific inhibitor from bench to bedside to treat human cancers.

Methods

Sex as a biological variable. For human samples, both male and female patients were included for lung and colon cancers, while prostate cancer samples were obtained from male patients and breast cancer samples from female patients. In animal studies, both male and female mice were used for the LLC1 lung cancer and MC38 colon cancer syngeneic models. For the 4T1 triple-negative breast cancer (TNBC) orthotopic syngeneic model, only female mice were used, whereas only male mice were used for the RM1 syngeneic tumor model.

Statistics. All sample numbers (n) represent biological replicates. Data are represented as the mean \pm SD, and error bars indicate standard deviation. Differences with P values less than 0.05 were considered significant. *P < 0.05, **P < 0.01, and ***P < 0.001. All analyses were performed using GraphPad Prism software (GraphPad Software, Inc.). student T test was used for comparisons of 2 groups. One-way ANOVA was used for comparisons among more than 2 groups. Two-way ANOVA was used for comparisons tumor growth and survival analysis.

Study approval. Human sample collection and use strictly followed the principles of the Declaration of Helsinki and were approved by the Institutional Review Board of the 920th Hospital of the Joint Logistics Support Force, Kunming, China (IRB#2020-035-01). All animal studies were conducted in accordance with protocols approved by the Institutional Animal Care and Use Committee of Northwestern University, Chicago, USA (IACUC#IS00029963). Written informed consent was obtained from all participants or their legal guardians. Detailed donor characteristics are provided in Supplemental Table 1.

Tumor model and maintenance of mice. BALB/c, C57BL/6, Rag1^{-/-}, and OT-I C57BL/6 mice were purchased

from Jackson laboratory and maintained in a specific pathogen-free facility. A total of 5×10⁵ RM1 or MC38 WT or USP22 KO cells were resuspended in 100 µL PBS and subcutaneously injected into the flank of C57BL/6 or Rag1^{-/-} mice aged at 7-8 weeks. A total of 5×10⁵ 4T-1 or 4T-1 R WT or USP22 KO cells were orthotopically injected into the mammary fat pad of BALB/c female mice aged at 7-8 weeks. Tumor volume was monitored every other day and calculated using the following formula: Tumor volume=length×width²/2. For the S02 treatment, 7-8 weeks C57BL/6 mice were subcutaneously inoculated with 5×10⁵ RM1 and MC38 cells. 24 hours later, mice were randomized into treatment groups. When the tumor volume reached around 50-100 mm³, mice were treated with S02 (10 mg/kg) and/or 100 μg PD-1 (Bio X Cell, BE0289) or IgG isotype antibody (Bio X Cell, BE0073), or vehicle control (10% DMSO) by intraperitoneal injection over 6 consecutive days. For 4T-1 cells, a total of 4T-1 WT or USP22 KO cells were orthotopically inoculated into the fourth MFP of 7-8 weeks female BALB/c mice. Mice were sacrificed by CO₂ asphyxiation followed by cervical dislocation. Post-mortem, tumors were immediately harvested and further processed for downstream experiments. For CD8⁺ T cell depletion assay, tumor bearing mice were intraperitoneally injected with 100 μg of αlgG2b (BioXCell, Cat# BE090) or αCD8 clone 2.43 (BioXCell, Cat# BE0061) in PBS when tumor volume reached around 50-100 mm³.

Lung cancer patients' recruitment and biopsy collection. Needle biopsies were collected from 32 newly diagnosed lung cancer patients (21 males and 11 females; mean age 59.4 years, range 44–71) prior to any therapy (immunotherapy, chemotherapy or radiotherapy). Patients were subsequently treated with anti-PD-1 as specified in Supplemental Table 1 and followed for at least three months after treatment. All human sample collection and use strictly adhered to the principles of the Declaration of Helsinki and were approved by the Clinical Study Review Board of the 920th Hospital of the Joint Logistics Support Force, Kunming, China (IRB#2020-035-01). Written informed consent was obtained from all participants or their legal guardians.

Tumor-infiltrating T cells in vitro re-stimulation. Tumor-bearing mice were sacrificed, and the tumors were harvested, photographed and processed for further analysis. Collected tumor tissues were cut into small pieces and digested with 1 mg/mL Collagenase D (Worthington, Cat#: LS004189) and 50 μg/mL DNase I (Roche, Cat#10104159001) with gentle shaking for 30 min at 37 °C. The digestion was stopped by EDTA (pH 8.0) and cells were filtered through 100 μm cell strainers. Following to incubate with ACK buffer (Fisher, catalog no. A1049201) to lyse red blood cells, a total of 5 × 10⁶ cells were stimulated with 2.5 mg/mL Phorbol 12-Myristate 13-Acetate (PMA) and 10 mg/mL ionomycin, and blocked with monensin (eBiosciences, Cat#00450551) for 2-3 hours at 37 °C. Cells were subjected to surface and intracellular staining as previously described in Flow Cytometry after washing twice with ice cold FACS buffer (PBS supplemented with 3% FBS). Indicated samples were evaluated on the BD LSRFortessaTM Cell Analyzer. All flow cytometry data were analyzed with FlowJo V10.8.1.

OT-I CD8⁺ T cell killing assay. Indicated RM1 or MC38 OVA expressing cells were seeded in a 96-well plate at a density of 1×10^5 per well. 4 hours after seeding, each well was gently washed twice with 100 μ L PBS. 1×10^5 freshly isolated splenic naïve OT-I CD8⁺ T were cultured in complete T cell media supplemented with 0.5 μ g/mL of anti-CD28 antibody. After culturing with CD8⁺ T cells for 48 hours, the supernatant of each well was carefully removed, and the cells were washed with PBS twice. Followed by fixation with 4% paraformaldehyde, adherent tumor cells were stained with 0.5 % crystal violet for 10 minutes at room temperature. After gently washing 6 times with PBS, the OD₄₅₀ values were evaluated by a spectrometer.

Tissue microarray. Tissue microarrays (TMA) with detailed clinical and pathological information were purchased and conducted by Shanghai YEPCOME Biotech Co., Ltd. The triple-negative breast cancer (TNBC) TMA included 163 samples, consisting of 133 breast cancer tissues and 30 adjacent healthy controls,

all from female patients (mean age 54.4 years, range 26–78). The prostate cancer TMA comprised 91 prostate cancer tissues and 53 matched para-tumor tissues, all from male patients (mean age 70.7 years, range 55–84). The colon cancer TMA contained 80 paired tumor and para-tumor tissues from 43 male and 37 female patients (mean age 66.5 years, range 31–88).

Immunohistochemistry. For immunohistochemical (IHC) staining, tissue specimens were deparaffinized in xylene, rehydrated through graded ethanol solutions, subjected to antigen retrieval and immersed in a 0.3% hydrogen peroxide solution. Slides were washed thrice with phosphate-buffered saline (PBS) and blocked with 5% bovine serum albumin for 30 min at room temperature. The tissue slides were subsequently incubated with primary antibodies overnight at 4 °C. HRP conjugated secondary antibody was used to incubate the slides before DAB detection. The quantification analysis of IHC results in multiplexed immunofluorescence.

Multiplexed Immunofluorescence (mIF). A multiplexed immunofluorescence (mIF) panel comprising β2M, USP22, EZH2 and CD8 $^{+}$, panCK and nuclear marker (DAPI), was developed. A TSA (tyramide signal amplification) approach was employed in multiplexed immunofluorescence staining according to our previous report (65). The staining procedure contained sequential cycles of antigen retrieval, non-specific antigen blocking, primary antibody incubation, secondary antibody incubation, and fluorescent labeling via TSA on whole slides. Briefly, tumor tissues were cut into 4 μm pieces and adhered to microscope slides. Tumor tissues were subsequently incubated with 3% H_2O_2 solution for 20 min. Sections were then incubated with 10% bovine serum albumin for 20 minutes at room temperature and incubated with antibodies at 4 $^{\circ}$ C overnight in the dark. Samples were rinsed three times with PBST (PBS supplemented with 0.2% Tween-20) before incubating with the indicated horseradish peroxidase (HRP) conjugated secondary antibody (1 μg/mL)

for 2 h at room temperature. This was followed by 3 washes with PBST and incubation with tyramide staining dye for 15 min at room temperature. Finally, the slides were counterstained with 1 μ g/ml DAPI (Life technology) for 5 min.

Quantification of mIF. USP22/EZH2/ β 2M expression were quantified specifically in panCK⁺ cells. Briefly, quantification analysis was double blindly performed using digital image analysis and spectral unmixing HALO software, which isolates individual panCK-positive cells and quantitatively measures USP22/EZH2/ β 2M expression in panCK-positive tumor cells. The panCK-negative CD8⁺ T cells were also quantified. For each case, random six fields (200 × 200 μ m per field), containing on average 200-250 cells per field, were analyzed. Quantification was performed using the following formula: H-Score = $\sum (pi \times i)$ = (percentage of negative cells × 0) + (percentage of weak-intensity cells × 1) + (percentage of moderate-intensity cells × 2) + (percentage of strong-intensity cells × 3). Here, 0, 1, 2, and 3 correspond to negative, weak, moderate, and strong expression, respectively, while pi and i represent the percentage of positive cells and the staining intensity, respectively. The percentage (pi) was automatically calculated using HALO software.

More information of methods can be found in supplemental information.

Data availability. The raw data is available to academic researchers from the corresponding author upon reasonable request. Values for all data points in graphs are reported in the Supporting Data Values file.

Author contributions

All authors read and approved of the final manuscript. D.Y.F. designed and supervised this project, and wrote the manuscript. K.L. performed most of the experiments and wrote the manuscript with input from Z.C.,

C.Y., W.Y., H.W. R.I., A.T., Q.G., N.L., B.G. edited the manuscript and analyzed the data. Y.L. and J.Z. collected the clinical NSCLC samples. D.M.W., S.K., W.J.G., H.L. revised the manuscript.

Acknowledgement

We thank Dr. Bin Zhang at Northwestern University for providing us with PC3 cells. K.L. was supported by the Robert H. Lurie Comprehensive Cancer Center of Northwestern University. This work was supported by National Institutes of Health (NIH) grants R01DK126908, R01DK120330, R01CA257520, R01CA284740 and CA232347 (to D.F.) and T32GM105538 and T32GM149439 (to A.Y.T.). This work is the result of NIH funding and is subject to the NIH Public Access Policy. Through acceptance of this federal funding, the NIH has been given a right to make the work publicly available in PubMed Central.

References

- 1. Jhunjhunwala S, Hammer C, and Delamarre L. Antigen presentation in cancer: insights into tumour immunogenicity and immune evasion. *Nature reviews Cancer*. 2021;21(5):298-312.
- 2. Sharma P, and Allison JP. Immune checkpoint therapy: Forging ahead. *Science translational medicine*. 2022;14(670):eadf2947.
- 3. Yang K, Halima A, and Chan TA. Antigen presentation in cancer mechanisms and clinical implications for immunotherapy. *Nature Reviews Clinical Oncology.* 2023;20(9):604-23.
- 4. Kim HJ, Cantor H, and Cosmopoulos K. Overcoming Immune Checkpoint Blockade Resistance via EZH2 Inhibition. *Trends Immunol.* 2020;41(10):948-63.
- 5. Pishesha N, Harmand TJ, and Ploegh HL. A guide to antigen processing and presentation. *Nature Reviews Immunology*. 2022;22(12):751-64.
- 6. Xu K, Wu ZJ, Groner AC, He HH, Cai C, Lis RT, et al. EZH2 oncogenic activity in castration-resistant prostate cancer cells is Polycomb-independent. *Science*. 2012;338(6113):1465-9.
- 7. Kim KH, and Roberts CWM. Targeting EZH2 in cancer. *Nature medicine*. 2016;22(2):128-34.
- 8. Burr ML, Sparbier CE, Chan KL, Chan YC, Kersbergen A, Lam EYN, et al. An Evolutionarily Conserved Function of Polycomb Silences the MHC Class I Antigen Presentation Pathway and Enables Immune Evasion in Cancer. *Cancer cell.* 2019;36(4):385-401.e8.
- 9. Cortez JT, Montauti E, Shifrut E, Gatchalian J, Zhang Y, Shaked O, et al. CRISPR screen in regulatory T cells reveals modulators of Foxp3. *Nature*. 2020;582(7812):416-20.
- 10. Zhou Y, Chu P, Wang Y, Li N, Gao Q, Wang S, et al. Epinephrine promotes breast cancer metastasis through a ubiquitin-specific peptidase 22-mediated lipolysis circuit. *Sci Adv.* 2024;10(33):eado1533.
- 11. Montauti E, Weinberg SE, Chu P, Chaudhuri S, Mani NL, Iyer R, et al. A deubiquitination module essential for T(reg) fitness in the tumor microenvironment. *Sci Adv.* 2022;8(47):eabo4116.
- 12. Casanova JL, MacMicking JD, and Nathan CF. Interferon-γ and infectious diseases: Lessons and prospects. *Science (New York, NY)*. 2024;384(6693):eadl2016.
- 13. Chen W, Khilko S, Fecondo J, Margulies DH, and McCluskey J. Determinant selection of major histocompatibility complex class I-restricted antigenic peptides is explained by class I-peptide affinity and is strongly influenced by nondominant anchor residues. *J Exp Med.* 1994;180(4):1471-83.
- 14. Met O, Buus S, and Claesson MH. Peptide-loaded dendritic cells prime and activate MHC-class I-restricted T cells more efficiently than protein-loaded cross-presenting DC. *Cell Immunol*. 2003;222(2):126-33.
- 15. Clarke SR, Barnden M, Kurts C, Carbone FR, Miller JF, and Heath WR. Characterization of the ovalbumin-specific TCR transgenic line OT-I: MHC elements for positive and negative selection. *Immunol Cell Biol.* 2000;78(2):110-7.
- 16. Matsushima S, Ajiro M, Iida K, Chamoto K, Honjo T, and Hagiwara M. Chemical induction of splice-neoantigens attenuates tumor growth in a preclinical model of colorectal cancer. *Science translational medicine*. 2022;14(673):eabn6056.
- 17. Lin Z, Tan C, Qiu Q, Kong S, Yang H, Zhao F, et al. Ubiquitin-specific protease 22 is a deubiquitinase of CCNB1. *Cell Discov.* 2015;1:15028-.
- 18. Lin Z, Yang H, Kong Q, Li J, Lee SM, Gao B, et al. USP22 antagonizes p53 transcriptional activation by deubiquitinating Sirt1 to suppress cell apoptosis and is required for mouse embryonic development. *Mol Cell*. 2012;46(4):484-94.
- 19. Gao Q, Li N, Pan Y, Chu P, Zhou Y, Jia H, et al. Hepatocyte growth factor promotes melanoma metastasis through ubiquitin-specific peptidase 22-mediated integrins upregulation. *Cancer Lett.* 2024:217196.
- 20. Liu K, Gao Q, Jia Y, Wei J, Chaudhuri SM, Wang S, et al. Ubiquitin-specific peptidase 22 controls

- integrin-dependent cancer cell stemness and metastasis. iScience. 2024;27(9):110592.
- 21. Lin ZH, Yang H, Kong QF, Li JP, Lee SM, Gao BX, et al. USP22 Antagonizes p53 Transcriptional Activation by Deubiquitinating Sirt1 to Suppress Cell Apoptosis and Is Required for Mouse Embryonic Development. *Molecular Cell*. 2012;46(4):484-94.
- 22. Melo-Cardenas J, Xu YM, Wei JC, Tan C, Kong SY, Gao BX, et al. USP22 deficiency leads to myeloid leukemia upon oncogenic Kras activation through a PU.1-dependent mechanism. *Blood.* 2018;132(4):423-34.
- 23. Kobayashi KS, and van den Elsen PJ. NLRC5: a key regulator of MHC class I-dependent immune responses. *Nature Reviews Immunology.* 2012;12(12):813-20.
- 24. Guirguis AA, Ofir-Rosenfeld Y, Knezevic K, Blackaby W, Hardick D, Chan YC, et al. Inhibition of METTL3 Results in a Cell-Intrinsic Interferon Response That Enhances Antitumor Immunity. *Cancer discovery.* 2023;13(10):2228-47.
- 25. Guan Q, Lin H, Miao L, Guo H, Chen Y, Zhuo Z, et al. Functions, mechanisms, and therapeutic implications of METTL14 in human cancer. *Journal of Hematology & Oncology.* 2022;15(1):13.
- 26. Blackledge NP, and Klose RJ. The molecular principles of gene regulation by Polycomb repressive complexes. *Nat Rev Mol Cell Bio.* 2021;22(12):815-33.
- 27. Piunti A, and Shilatifard A. The roles of Polycomb repressive complexes in mammalian development and cancer. *Nat Rev Mol Cell Bio.* 2021;22(5):326-45.
- 28. Ennishi D, Takata K, Béguelin W, Duns G, Mottok A, Farinha P, et al. Molecular and Genetic Characterization of MHC Deficiency Identifies EZH2 as Therapeutic Target for Enhancing Immune Recognition. *Cancer discovery.* 2019;9(4):546-63.
- 29. Burr ML, Sparbier CE, Chan KL, Chan YC, Kersbergen A, Lam EYN, et al. An Evolutionarily Conserved Function of Polycomb Silences the MHC Class I Antigen Presentation Pathway and Enables Immune Evasion in Cancer. *Cancer Cell.* 2019;36(4):385-401 e8.
- 30. Cruz Walma DA, Chen Z, Bullock AN, and Yamada KM. Ubiquitin ligases: guardians of mammalian development. *Nature Reviews Molecular Cell Biology.* 2022;23(5):350-67.
- 31. Gregory S, Xu Y, Xie P, Fan J, Gao B, Mani N, et al. The ubiquitin-specific peptidase 22 is a deubiquitinase of CD73 in breast cancer cells. *American journal of cancer research*. 2022;12(12):5564-75.
- 32. Pusztai L, Yau C, Wolf DM, Han HS, Du L, Wallace AM, et al. Durvalumab with olaparib and paclitaxel for high-risk HER2-negative stage II/III breast cancer: Results from the adaptively randomized I-SPY2 trial. *Cancer cell.* 2021;39(7):989-98.e5.
- 33. Riaz N, Havel JJ, Makarov V, Desrichard A, Urba WJ, Sims JS, et al. Tumor and Microenvironment Evolution during Immunotherapy with Nivolumab. *Cell.* 2017;171(4):934-49.e16.
- 34. Limagne E, Nuttin L, Thibaudin M, Jacquin E, Aucagne R, Bon M, et al. MEK inhibition overcomes chemoimmunotherapy resistance by inducing CXCL10 in cancer cells. *Cancer cell.* 2022;40(2):136-52.e12.
- 35. Bernal M, Garcia-Alcalde F, Concha A, Cano C, Blanco A, Garrido F, et al. Genome-wide differential genetic profiling characterizes colorectal cancers with genetic instability and specific routes to HLA class I loss and immune escape. *Cancer Immunol Immunother*. 2012;61(6):803-16.
- 36. Li J, Yuan S, Norgard RJ, Yan F, Yamazoe T, Blanco A, et al. Tumor Cell-Intrinsic USP22 Suppresses Antitumor Immunity in Pancreatic Cancer. *Cancer immunology research*. 2020;8(3):282-91.
- 37. Chen X, Lu Q, Zhou H, Liu J, Nadorp B, Lasry A, et al. A membrane-associated MHC-I inhibitory axis for cancer immune evasion. *Cell.* 2023;186(18):3903-20 e21.
- 38. Bao Y, Cruz G, Zhang Y, Qiao Y, Mannan R, Hu J, et al. The UBA1-STUB1 axis mediates cancer immune escape and resistance to checkpoint blockade. *Cancer Discov.* 2024.
- 39. Tan L, Yin T, Xiang H, Wang L, Mudgal P, Chen J, et al. Aberrant cytoplasmic expression of UHRF1

- restrains the MHC-I-mediated anti-tumor immune response. Nat Commun. 2024;15(1):8569.
- 40. van de Weijer ML, Samanta K, Sergejevs N, Jiang L, Duenas ME, Heunis T, et al. Tapasin assembly surveillance by the RNF185/Membralin ubiquitin ligase complex regulates MHC-I surface expression. *Nat Commun.* 2024;15(1):8508.
- 41. Xiong W, Gao X, Zhang T, Jiang B, Hu MM, Bu X, et al. USP8 inhibition reshapes an inflamed tumor microenvironment that potentiates the immunotherapy. *Nat Commun.* 2022;13(1):1700.
- 42. Liu H, Wilson KR, Firth AM, Macri C, Schriek P, Blum AB, et al. Ubiquitin-like protein 3 (UBL3) is required for MARCH ubiquitination of major histocompatibility complex class II and CD86. *Nat Commun.* 2022;13(1):1934.
- 43. Huang J, Yin Q, Wang Y, Zhou X, Guo Y, Tang Y, et al. EZH2 Inhibition Enhances PD-L1 Protein Stability Through USP22-Mediated Deubiquitination in Colorectal Cancer. *Advanced science* (Weinheim, Baden-Wurttemberg, Germany). 2024;11(23):e2308045.
- 44. Xiao G, Jin LL, Liu CQ, Wang YC, Meng YM, Zhou ZG, et al. EZH2 negatively regulates PD-L1 expression in hepatocellular carcinoma. *Journal for immunotherapy of cancer.* 2019;7(1):300.
- 45. Zhao Y, Wang XX, Wu W, Long H, Huang J, Wang Z, et al. EZH2 regulates PD-L1 expression via HIF-1α in non-small cell lung cancer cells. *Biochemical and biophysical research communications*. 2019;517(2):201-9.
- 46. Cohen R, Colle R, Pudlarz T, Heran M, Duval A, Svrcek M, et al. Immune Checkpoint Inhibition in Metastatic Colorectal Cancer Harboring Microsatellite Instability or Mismatch Repair Deficiency. *Cancers (Basel)*. 2021;13(5).
- 47. Shan T, Chen S, Wu T, Yang Y, Li S, and Chen X. PD-L1 expression in colon cancer and its relationship with clinical prognosis. *Int J Clin Exp Pathol.* 2019;12(5):1764-9.
- 48. Mok TSK, Wu YL, Kudaba I, Kowalski DM, Cho BC, Turna HZ, et al. Pembrolizumab versus chemotherapy for previously untreated, PD-L1-expressing, locally advanced or metastatic non-small-cell lung cancer (KEYNOTE-042): a randomised, open-label, controlled, phase 3 trial. *Lancet*. 2019;393(10183):1819-30.
- 49. Takahashi M, Cortes J, Dent R, Pusztai L, McArthur H, Kummel S, et al. Pembrolizumab Plus Chemotherapy Followed by Pembrolizumab in Patients With Early Triple-Negative Breast Cancer: A Secondary Analysis of a Randomized Clinical Trial. *JAMA Netw Open.* 2023;6(11):e2342107.
- 50. Huang X, Zhang Q, Lou Y, Wang J, Zhao X, Wang L, et al. USP22 Deubiquitinates CD274 to Suppress Anticancer Immunity. *Cancer Immunol Res.* 2019;7(10):1580-90.
- 51. Huang P, Zhou X, Zheng M, Yu Y, Jin G, and Zhang S. Regulatory T cells are associated with the tumor immune microenvironment and immunotherapy response in triple-negative breast cancer. *Front Immunol.* 2023;14:1263537.
- 52. Zahran AM, El-Badawy O, Kamel LM, Rayan A, Rezk K, and Abdel-Rahim MH. Accumulation of Regulatory T Cells in Triple Negative Breast Cancer Can Boost Immune Disruption. *Cancer Manag Res.* 2021;13:6019-29.
- 53. Malla RR, Vasudevaraju P, Vempati RK, Rakshmitha M, Merchant N, and Nagaraju GP. Regulatory T cells: Their role in triple-negative breast cancer progression and metastasis. *Cancer.* 2022;128(6):1171-83.
- 54. Spranger S, and Gajewski TF. Impact of oncogenic pathways on evasion of antitumour immune responses. *Nature reviews Cancer.* 2018;18(3):139-47.
- 55. Dhatchinamoorthy K, Colbert JD, and Rock KL. Cancer Immune Evasion Through Loss of MHC Class I Antigen Presentation. *Frontiers in immunology.* 2021;12:636568.
- 56. Glinsky GV, Berezovska O, and Glinskii AB. Microarray analysis identifies a death-from-cancer signature predicting therapy failure in patients with multiple types of cancer. *J Clin Invest.* 2005;115(6):1503-21.

- 57. Lahad JP, Mills GB, and Coombes KR. Stem cell-ness: a "magic marker" for cancer. *The Journal of clinical investigation*. 2005;115(6):1463-7.
- 58. Lin Z, Yang H, Kong Q, Li J, Lee SM, Gao B, et al. USP22 antagonizes p53 transcriptional activation by deubiquitinating Sirt1 to suppress cell apoptosis and is required for mouse embryonic development. *Molecular Cell.* 2012;46(4):484-94.
- 59. Liu H, Liu N, Zhao Y, Zhu X, Wang C, Liu Q, et al. Oncogenic USP22 supports gastric cancer growth and metastasis by activating c-Myc/NAMPT/SIRT1-dependent FOXO1 and YAP signaling. *Aging*. 2019;11(21):9643-60.
- 60. Gennaro VJ, Stanek TJ, Peck AR, Sun Y, Wang F, Qie S, et al. Control of CCND1 ubiquitylation by the catalytic SAGA subunit USP22 is essential for cell cycle progression through G1 in cancer cells. *Proc Natl Acad Sci U S A*. 2018;115(40):E9298-E307.
- 61. Zhang XY, Varthi M, Sykes SM, Phillips C, Warzecha C, Zhu W, et al. The putative cancer stem cell marker USP22 is a subunit of the human SAGA complex required for activated transcription and cell-cycle progression. *Mol Cell.* 2008;29(1):102-11.
- 62. Atanassov BS, Evrard YA, Multani AS, Zhang Z, Tora L, Devys D, et al. Gcn5 and SAGA regulate shelterin protein turnover and telomere maintenance. *Mol Cell*. 2009;35(3):352-64.
- 63. Kosinsky RL, Helms M, Zerche M, Wohn L, Dyas A, Prokakis E, et al. USP22-dependent HSP90AB1 expression promotes resistance to HSP90 inhibition in mammary and colorectal cancer. *Cell Death Dis.* 2019;10(12):911.
- 64. Melo-Cardenas J, Zhang Y, Zhang DD, and Fang D. Ubiquitin-specific peptidase 22 functions and its involvement in disease. *Oncotarget*. 2016;7(28):44848-56.
- 65. Liu K, Jiang L, Shi Y, Liu B, He Y, Shen Q, et al. Hypoxia-induced GLT8D1 promotes glioma stem cell maintenance by inhibiting CD133 degradation through N-linked glycosylation. *Cell Death & Differentiation*. 2022;29(9):1834-49.

Figure and figure legends

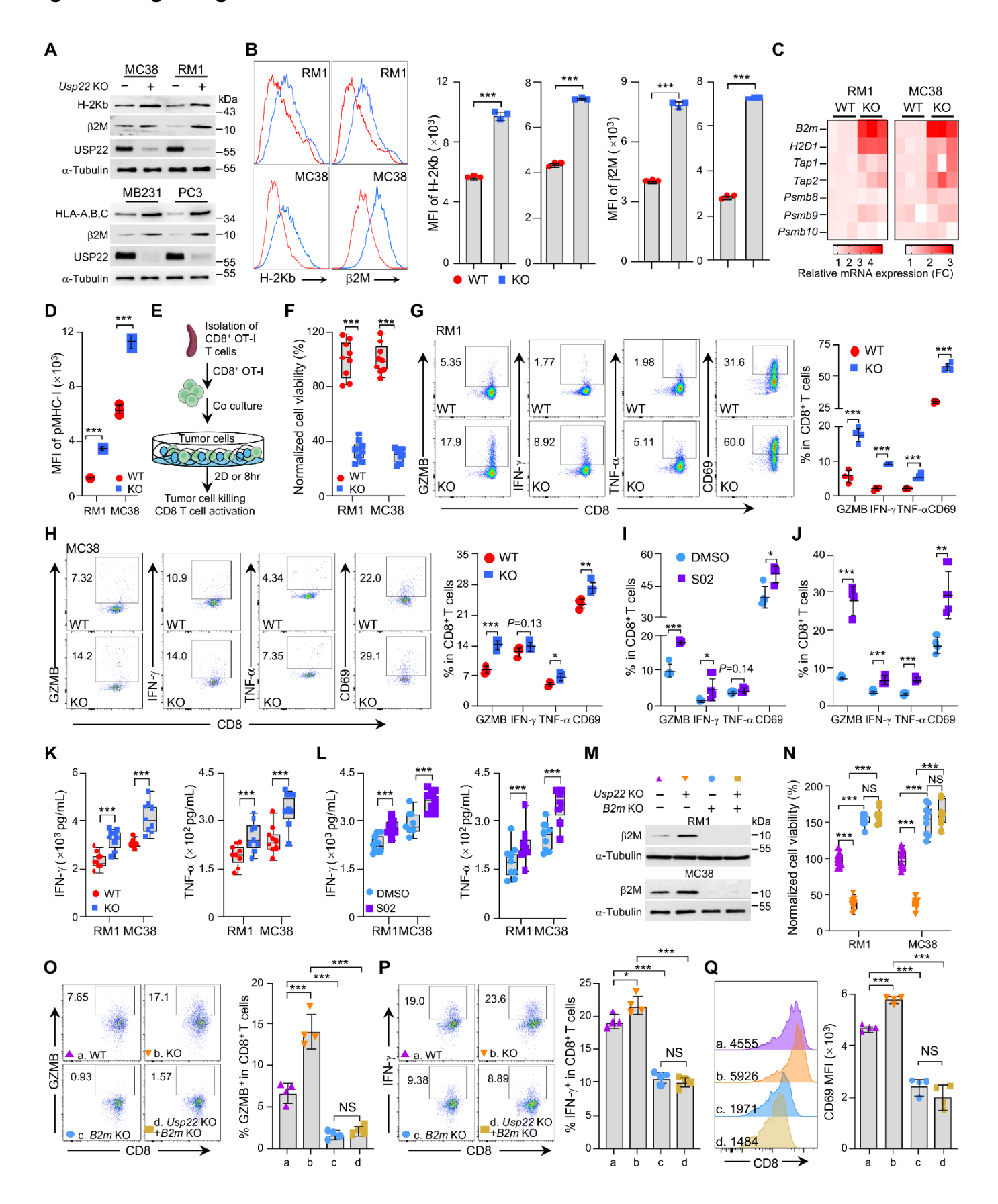


Figure 1. Usp22 inhibition enhances MHC-I expression. Indicated cells were transfected with control

(WT) or Usp22-specific guide RNAs (Usp22 KO). (A) Immunoblot analysis of MHC-I proteins in WT and Usp22 KO tumor cells. (B) Cell surface expression of H-2Kb and β2M were determined in WT and Usp22 KO cells. (C) Heatmap summarizing for the mRNA expression of genes involved in antigen presentation in WT and KO tumor cells. (D) Cell surface levels of OVA peptide SIINFEKL (pMHC-I) were determined in WT and Usp22 KO MC38/OVA or RM1/OVA cells. (E) Schematic illustration of an in vitro cytotoxicity assay. (F) The viability of WT and Usp22 KO MC38/OVA or RM1/OVA after co-cultured with OT-I CD8⁺ T cells. (G and H) OT-I CD8⁺ T cell activation after co-cultured with WT and Usp22 KO RM1/OVA or MC38/OVA cells were determined. (I and J) RM1/OVA (I) or MC38/OVA (J) cells were pre-treated with or without 20 μM USP22i-S02 for 48 h and then co-cultured with OT-I CD8⁺ T cells. OT-I CD8⁺ T cell activation was determined as in (I-J). (K) WT and Usp22 KO RM1/OVA or MC38/OVA cells were co-cultured with OT-I CD8 T cells. The concentrations of IFN- γ or TNF- α in the supernatant were determined by ELISA (N=9). (L) RM1/OVA or MC38/OVA cells were pretreated with USPi-S02 as in (I) and then co-cultured with OT-I cells. The concentrations of IFN- γ and TNF- α in the supernatant were determined by ELISA (N=9). (M) B2m was deleted by CRISPR in WT and Usp22 KO MC38/OVA and RM1/OVA cells. (N-Q) The effect of B2m deletion on CD8mediated killing of tumor cells (N) and OT-I CD8 T cell activation was determined as in (P-Q). Statistics were calculated by unpaired two-tailed t-test (B, D, F-L) or one-way analysis of variance (ANOVA) followed by Tukey's test (N-Q).

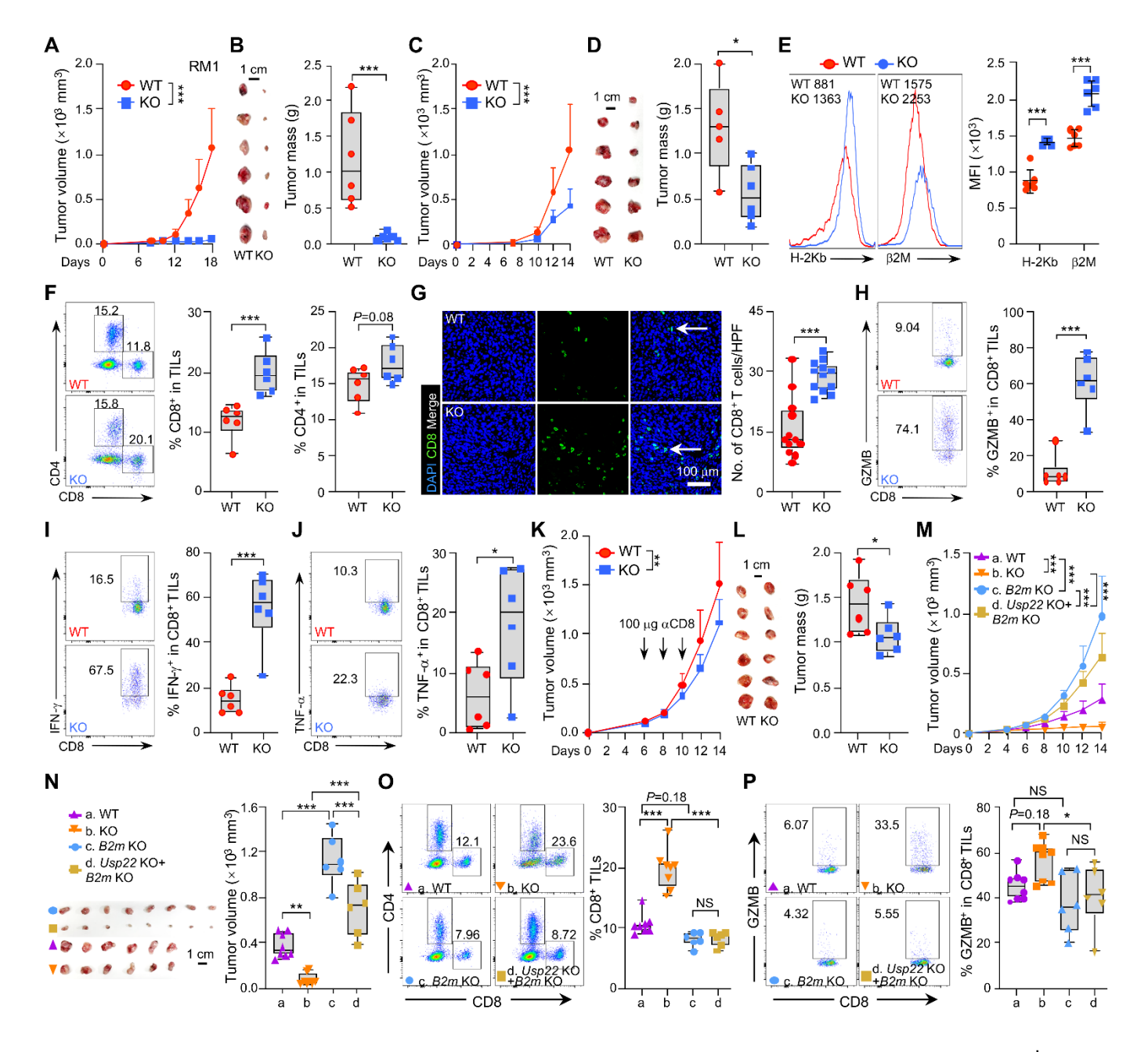


Figure 2. The absence of Usp22 dampens tumor growth by enhancing tumoral infiltrating CD8⁺ T cells.

(A and B). Effect of *Usp22* depletion on tumorigenesis of RM1 cells in C57BL/6 mice. Tumor volume (A), endpoint tumor images and weight (B) are shown. Scale bar: 1 cm. (C and D) Effect of *Usp22* depletion on tumorigenesis of RM1 cells in immunocompromised RAG1 knockout mice were determined as in (A and B), Scale bars: 1 cm. (E) Flow cytometric analysis of the expression of H-2Kb or β 2M on tumoral cells in (A). (F-G) Tumoral infiltrating CD4⁺ and CD8⁺ T cells on the total CD45⁺ cells in tumors shown in (A) were analyzed by flow cytometry (F) or immunofluorescence staining (G). Scale bar: 100 μ m. HPF, high powered field. (H-J) The production of granzyme B⁺ (H), IFN- γ ⁺ (I) or TNF- α ⁺ (J) by CD8⁺ in (F). (K and L) Tumor-bearing mice

were treated with CD8 depleting antibodies (100 μg) on day 6, 9 and 12. Tumor volume (K), endpoint tumor images and weight (L) were recorded. Scale bar: 1 cm. (M and N) WT, *Usp22* KO, *B2m* KO or double KO (dKO) RM1 cells were subcutaneously injected into C57BL/6 mice, tumor volume (M), endpoint tumor images and weight (N) are shown. scale bar: 1 cm. (O and P) Tumoral infiltrating CD8⁺ T cells (O) or their production of GZMB (P) were analyzed. Statistics were calculated by unpaired two-tailed t-test (B, D, E-J, L) or one-way ANOVA followed by Tukey's test (N-P). Two-way ANOVA with multiple comparisons (A, C, K, M).

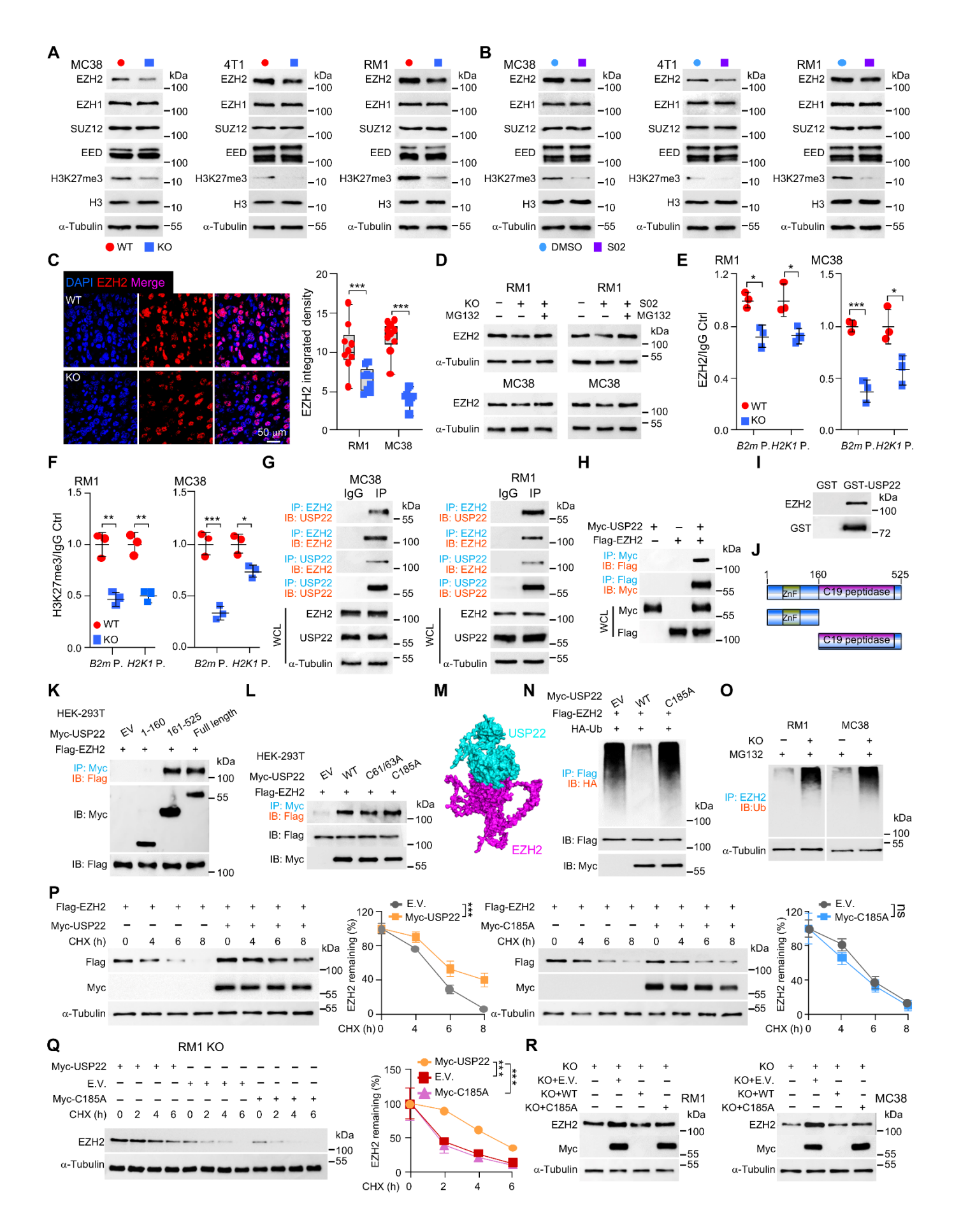


Figure 3. USP22 is an EZH2-specific deubiquitinase. (A and B) Immunoblot analysis of indicated protein

levels in WT and KO tumor cells (A) or in tumor cells treated with 20 μM USP22i-S02 (B). (C) Immunofluorescence staining and quantification of EZH2 in WT and KO RM1 tumors. Scale bars, 50 μm. (D) Immunoblot analysis of indicated protein levels in WT and KO cells treated with or without MG132 (10 μM, 8 hours). (E and F) Ch-IP and qRT-PCR analysis for EZH2 (E), H3K27me3 (F) enrichment in B2m or H-2K1 genes promoter in WT and KO cells. (G) Analysis of USP22 interaction with PCR2 complex proteins by Co-IP and immunoblot. WCL: whole cell lysates. (H) Analysis of USP22 interaction with EZH2 in transiently transfect HEK-293T cells. (I) Recombinant GST/GST-USP22 were purified from bacteria and incubated with 4T1 cell lysate overnight. The binding proteins were analyzed by immunoblot. (J) Schematic illustration of USP22 and its truncated mutants. (K and L) Analysis of EZH2 interaction with USP22 and its mutants in transiently transfected HEK-293T cells. (M) Molecular docking analysis of the interaction between USP22 and EZH2. (N) EZH2 ubiquitination was determined HEK293T cells in the presence of transient transfection of Myc-USP22/C185A, HA-ubiquitin. (O) Indicated cells were pre-treated with 10 μM MG132 for 8 hours, EZH2 ubiquitination was determined. (P) HEK-293T cells co-transfected with FLAG-EZH2 and Myc-USP22 or its C185A mutant. After 24 hours transfection, cells were treated with 20 mg/mL cycloheximide (CHX) for the indicated timepoints and indicated protein levels were determined. (Q) RM1 KO cells were transfected with Usp22/C185A mutant. EZH2 protein stability was determined as in (P). (R) EZH2 protein stability in WT and KO RM1 and MC38 cells were determined as in (P). Statistics were calculated by unpaired two-tailed ttest (C, E, F) or two-way ANOVA with multiple comparisons (P, Q).

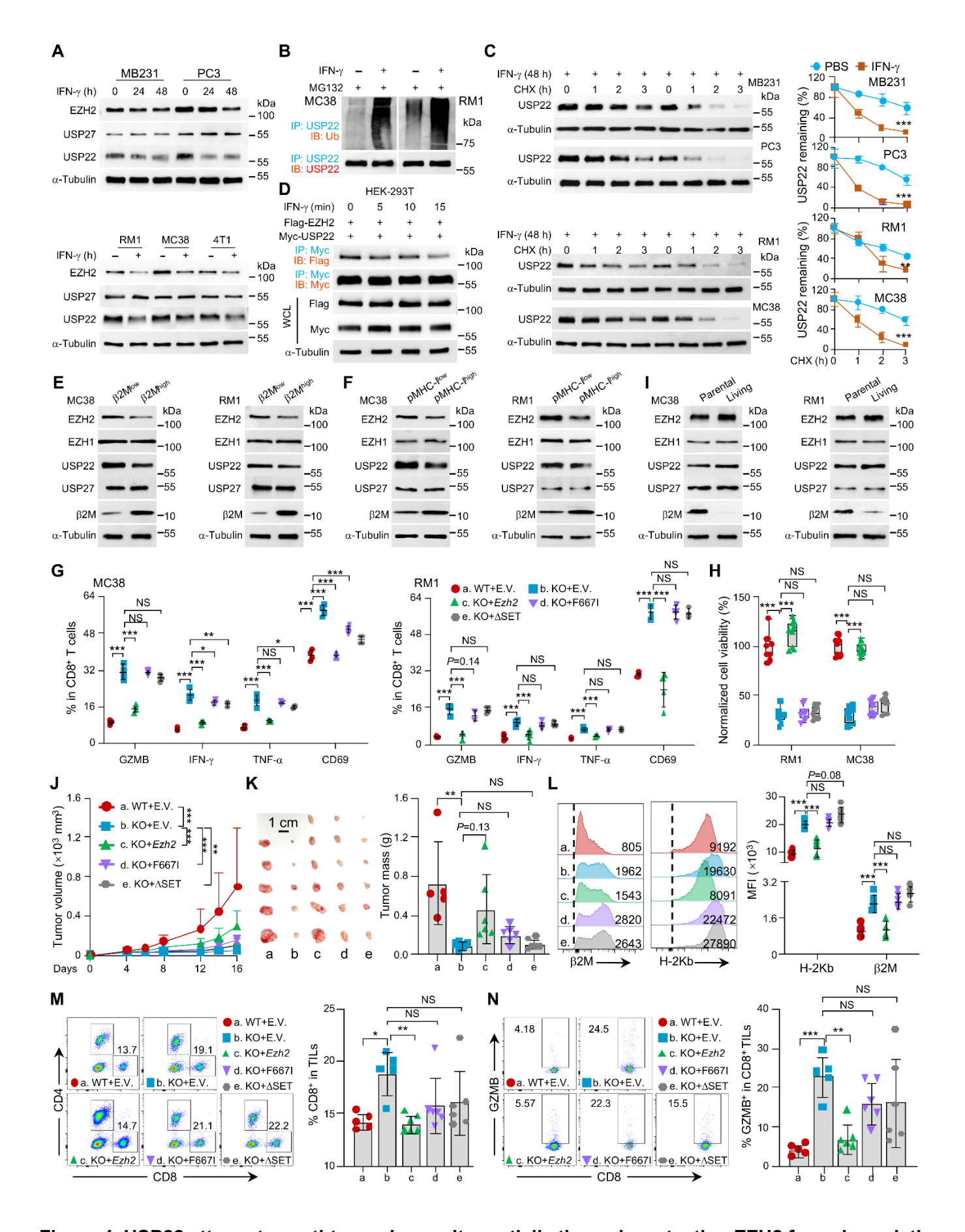


Figure 4. USP22 attenuates anti-tumor immunity partially through protecting EZH2 from degradation.

(A-C) Each indicated cancer cells were treated with 10 ng/mL IFN-γ for indicated timepoints. The expression of indicated proteins was determined. (D) HEK-293T cells were co-transfected with FLAG-EZH2 and Myc-USP22 and then treated with 10 ng/mL IFN-γ for the indicated times. The interaction between USP22 and EZH2 was determined. (E) Tumor cells were isolated based on membrane β2M expression. Indicated protein expression was determined. (F) MC38/OVA or RM1/OVA were isolated according to cell surface pMHC-I. Indicated protein expression was determined. (G) OT-I CD8⁺ T cells were isolated from OT-I mice and cocultured with Usp22-deficient RM1/OVA or MC38/OVA cells with or without Ezh2, Ezh2 F667I or ΔSET mutant reconstitution for 8 hours at the ratio of 1:1 in the presence of CD28 blocking antibodies treatment. Quantification data of flow cytometric analysis of percentages of GZMB⁺, IFN- γ ⁺ and TNF- α ⁺ producing CD8⁺ T cells are shown. (H) Cell viability of indicated cells after co-culturing for 48 hours. (I) Living tumor cells were collected after co-cultured with naïve OT-I CD8⁺ T cells for 48 hours at a ratio of 1:1 in the presence of CD28 blocking antibodies treatment. Indicated protein levels were determined. (J-K) MC38 cells with Ezh2, Ezh2 F667I, or \triangle SET mutant reconstitution in the setting of *Usp22* depletion were inoculated into immunocompetent mice. Tumor volume (J) and endpoint mass (K) of indicated tumors were recorded. (L) The expression of β2M and H-2Kb on indicated tumor cell surface. (M-N) The frequencies of tumoralinfiltrating CD8⁺ T cells (M) or GZMB⁺ producing CD8⁺ T cells (N) from indicated MC38 tumors. Statistics were calculated by one-way ANOVA followed by Tukey's test (G, H, K-N). Two-way ANOVA with multiple comparisons (C, J).

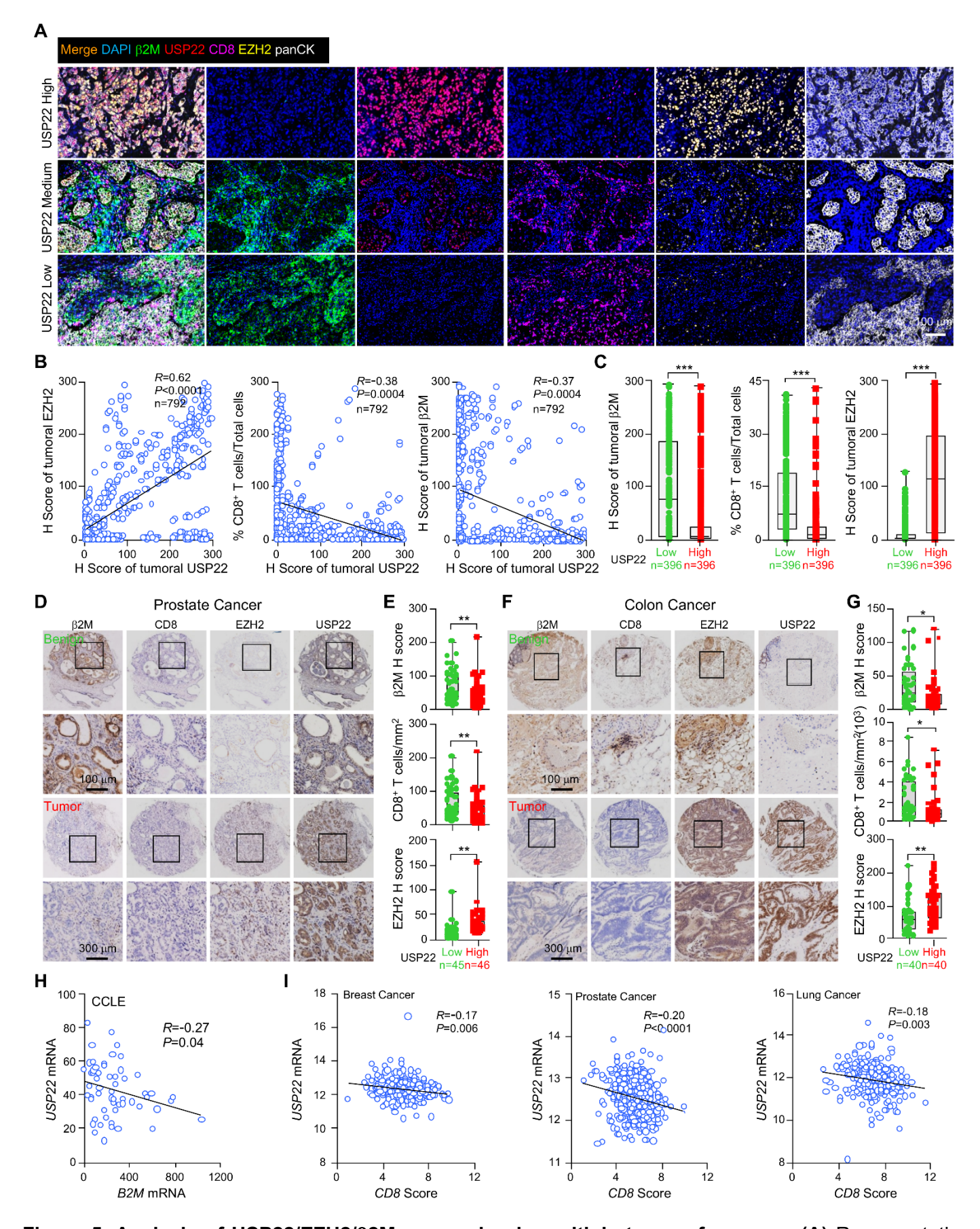


Figure 5. Analysis of USP22/EZH2/β2M expression in multiple types of cancers. (A) Representative images of multiplexed immunofluorescence staining of USP22/EZH2/β2M/CD8 in breast cancer tissues with

different USP22 intensity. Scale bar, 100 μm. H-score, histochemical scoring assessment. (B) The correlation between USP22 with β2M, USP22 with CD8, and USP22 with EZH2. (C) Quantification of tumoral-infiltrated CD8⁺ T cells, EZH2, or β2M intensity in breast cancer tissues with different USP22 intensity. Patients were classified into the USP22 intensity low or high group. The median value was used as cutoff. (D) Immunohistochemical staining of USP22/EZH2/β2M/CD8 in a prostate cancer tissue microarray. Scale bar: 200 μ m. (E) The proportion of tumor-infiltrating CD8⁺ T cells or β 2M and EZH2 intensity in different intensity cohorts. Patients were classified into the USP22 intensity low or high group. The median value was used as cutoff. (F) Immunohistochemical staining of USP22/EZH2/β2M/CD8 in colorectal tissue microarray containing 80 paired benign or colorectal cancer tissues. Scale bar: 200 μm. (G) The proportion of tumoral-infiltrated CD8⁺ T cells or β2M and EZH2 intensity in low or high USP22 intensity cohorts. Patients were classified into the USP22 intensity low or high group. The median value was used as cutoff. (H) Correlations between the mRNA levels of USP22 and B2M in breast cancer cell lines from Cancer Cell Line Encyclopedia (CCLE). (I) Correlations between the mRNA expression of USP22 and CD8 infiltration score in prostate or colorectal cancer from TCGA database. Statistics were calculated by unpaired two-tailed t-test (C, E, G), two-tailed Pearson correlation-test (B, H, I).

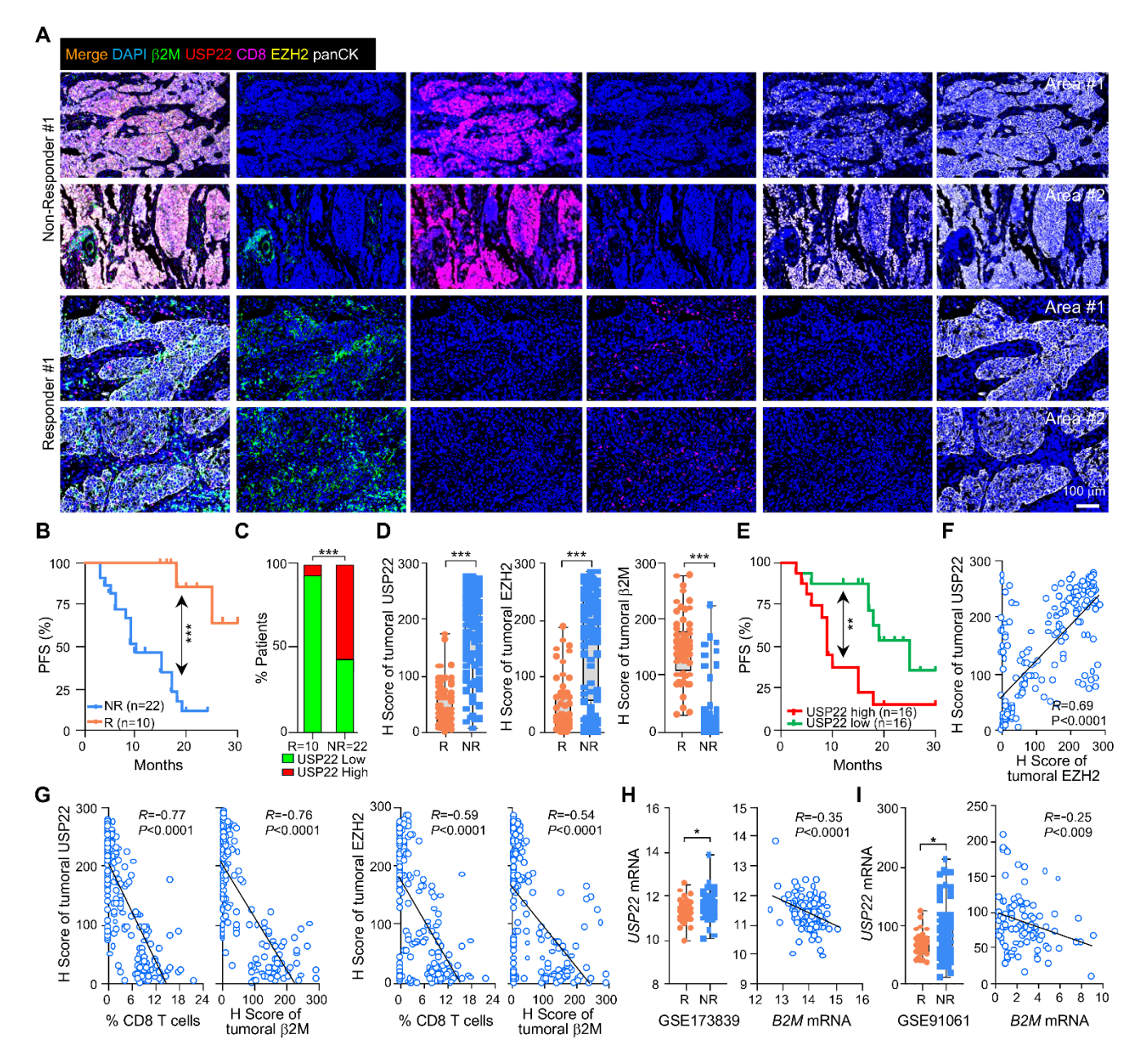


Figure 6. USP22 expression links with ICB resistance. (A) Representative images of multiplexed immunofluorescence staining of USP22/EZH2/β2M/CD8 in 32 pretreatment biopsies taken from individual patients who received αPD-1 antibody therapy. Scale bar, 100 μm. (B) Kaplan-Meier plot of progression-free survival (PFS) for 32 patients with NSCLC who did or did not respond to αPD-1 antibody therapy. (C) Patients were divided into USP22 low or high groups according to USP22 expression. Frequency of responder or non-responder with high or low USP22 expressions are shown. R. and NR. indicate responders and non-responders, respectively. (D) Quantification data of USP22/EZH2/β2M intensity in biopsies from αPD-1 responders or non-responders. (E) Kaplan-Meier plot of PFS for patients treated with αPD-1 in USP22 low

versus high group. Patients were classified into the USP22 low or high groups, with the median expression value across all the samples used as the cutoff. **(F-G)** Pearson correlation analyses between indicated proteins expression in biopsies from patients who did or did not respond to α PD-1 therapy. **(H)** The mRNA expression of *USP22* in pretreatment biopsies from patients with triple negative breast cancer who received α PD-1 therapy. Clinical responses were classified in the original studies GSE173839. Correlations between the mRNA expression of *USP22* and *B2M* are shown. **(I)** The mRNA expression of *USP22* in pretreatment biopsies with melanoma who received α PD-1 therapy. Clinical responses were classified in the original studies GSE91061. Correlations between the mRNA expression of *USP22* and *B2M* are shown. Statistics were calculated by unpaired two-tailed t-test (D, H-I (left panel)), Fisher exact test (C), Log rank t test (B, E), two-tailed Pearson correlation-test (F, G, H-I (right panel)).

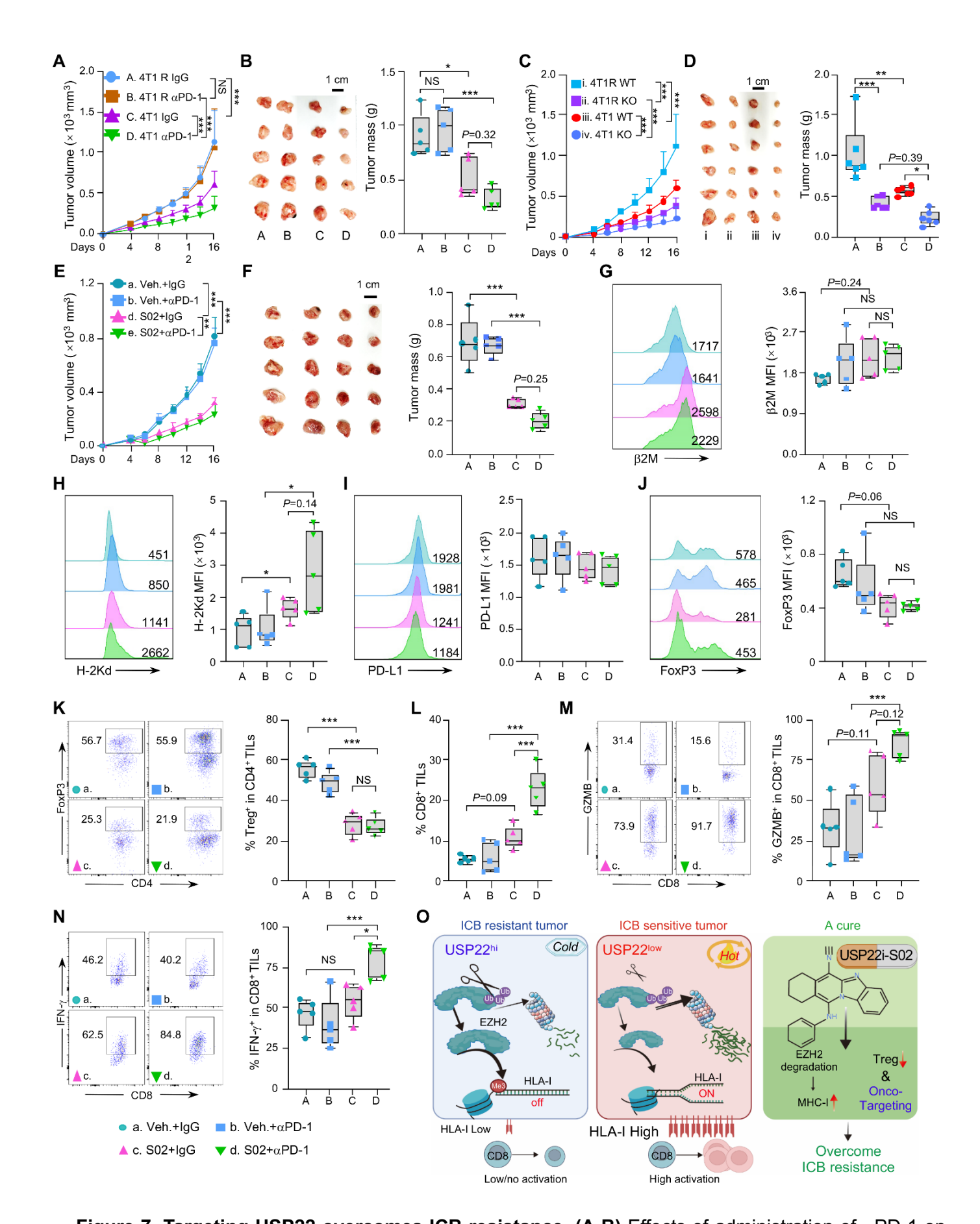


Figure 7. Targeting USP22 overcomes ICB resistance. (A-B) Effects of administration of α PD-1 on 4T1 or 4T1R tumors growth (A) and weight (B). Image of 4T1 or 4T1 R tumors treated with or without α PD-

1 are shown. **(C-D)** Effects of *Usp22* deficiency on 4T1 or 4T1R tumors growth (C) and weight (D). **(E-F)** Effects of S02 or αPD-1 in 4T-1 R tumor growth. Mice were randomly grouped into 4 groups and administered with 10 mg/kg USP22i-S02 and/or 100 μg αPD-1. Green or purple arrows indicate administration αPD-1 or S02, respectively. **(G-I)** Representative flow cytometric images and quantification data of cell surface β2M (G), H-2Kd (H) or PD-L1 (I) MFI in indicated tumor cells. **(J)** Representative flow cytometric images and quantification of FoxP3 MFI. **(K)** Representative images of flow cytometric analysis and quantification of frequencies of Tregs cells among total CD4* lymphocytes in indicated tumors. **(L)** Quantification of frequencies of CD8* T cells among tumor-infiltrating CD45* lymphocytes in indicated tumors. **(M-N)** Representative flow cytometric images and quantification of frequencies of GZMB (M) or IFN-γ (N) producing tumor-infiltrating CD8* T cells in indicated tumors. **(O)** Proposed working model showing that USP22 inhibition enhances anti-tumor immunity through increases EZH2 proteasomal mediated degradation and MHC-I medicated CD8* T cells recognition and killing. Pharmacological USP22 inhibition overcomes immune checkpoint blockade resistance. Statistics were calculated by one-way ANOVA followed by Tukey's test (B, D, F-N) or two-way ANOVA with multiple comparisons (A, C, E).